공학석사학위논문

압전 에너지 하베스팅의 전력 예측을 위한 수학적 해석 모델 개발

Analytical Model for Electric Power Prediction of Piezoelectric Energy Harvesting

2013 년 2 월

서울대학교 대학원

기계항공공학부

윤 헌 준

압전 에너지 하베스팅의 전력 예측을 위한 수학적 해석 모델 개발

Analytical Model for Electric Power Prediction of Piezoelectric Energy Harvesting

지도교수 윤 병 동

이 논문을 공학석사 학위논문으로 제출함

2013 년 2 월

서울대학교 대학원

기계항공공학부

윤 헌 준

윤헌준의 공학석사 학위논문을 인준함

2012 년 12 월

위 원 장 신 효 철 (인)

부위원장 윤 병 동 (인)

위 원 조 맹 효 (인)

Abstract

Analytical Model for Electric Power Prediction of Piezoelectric Energy Harvesting

Heonjun Yoon
School of Mechanical and Aerospace Engineering
The Graduate School
Seoul National University

Vibration energy can be converted into electrical energy using a piezoelectric energy harvester. An analytical model is of great importance to understand the first principle of piezoelectric energy conversion mechanism. Furthermore, for quick decision-making of the number and location of piezoelectric energy harvesters, harvestable electric power must be analytically quantified under a given vibration condition. In order to develop the analytical model for electric power prediction of the piezoelectric energy harvester, this study aims at advancing two essential research areas: 1) research thrust 1 – stochastic electric power prediction under non-stationary random vibrations, 2) research thrust 2 – the electromechanically coupled analytical model of an energy harvesting skin (EH skin).

In research thrust 1, statistical time-frequency analysis, smoothed pseudo Wigner-Ville distribution, was used to estimate a time-varying power spectral density (time-varying PSD) of a non-stationary random vibration signal. The time-varying PSD of the output voltage response was estimated from a linear electromechanical operator. Finally the expected electric power was obtained from the autocorrelation function which is the inverse Fourier transform of the time-varying PSD of the output voltage.

In research thrust 2, the electromechanically analytical model of the EH skin was developed using the Kirchhoff plate theory. The Levy solution was used to calculate the natural frequencies and mode shapes. A steady-state output voltage response was obtained by solving the mechanical equation of motion and electrical circuit equation simultaneously. The analytical plate model can be also used for EH skin design to extract the inflection lines for piezoelectric material segmentation to avoid the voltage cancellation.

Keywords: Piezoelectric Energy Harvesting
Non-Stationary Random Vibrations
Statistical Time-Frequency Analysis
Time-Varying Power Spectral Density
Kirchhoff Plate Theory
Piezoelectric Material Segmentation

Student Number: 2011-20730

Table of Contents

List of Tables

List of Figures

Nomenclatures

a	length of the piezoelectric energy harvester
b	width of the piezoelectric energy harvester
c_{11}^{E}	elastic modulus of the piezoelectric layer
C_p	capacitance
D	electric displacement component
d	piezoelectric strain coefficient
E	electric field
$E[P(t)]$	expected electric power
$\overline{e}$	piezoelectric constant
ε_0	absolute permittivity
ε_{33}^{S}	relative permittivity at constant strain
ε_{33}^{T}	relative permittivity at constant stress
ϕ	$= b/a$, aspect ratio
ζ	modal damping ratio
η	$= y/b$, dimensionless coordinate
$H(\omega)$	linear operator
h_p	thickness of the piezoelectric layer
h_{pc}	distance from the center of the piezoelectric layer to the neutral axis

h_s	thickness of the substrate layer
λ	eigenvalue
ν_p	Poisson's ratio of piezoelectric layer
ν_s	Poisson's ratio of substrate layer
ζ	= x / a , dimensionless coordinate
R_{load}	external resistance
ρ_p	density of the piezoelectric layer
ρ_s	density of the substrate layer
S	strain component
$S_v(t,\omega)$	time-varying PSD of the output voltage response
$S_X(t,\omega)$	time-varying PSD of the input random vibration
T	stress component
τ	time-lag of the autocorrelation function
$v(t)$	output voltage response
Y_s	elastic modulus of the substrate layer

Chapter 1. Introduction

1.1 Motivation

The advances in wireless communications and low-power technology promote the use of wireless sensors. However, the limited life expectancy and high replacement cost of batteries make it difficult to use wireless sensors, although they have lots of benefits more than wired sensors. Energy harvesting (EH) technology, which scavenges electric power from ambient, otherwise wasted, energy sources, has been emerged as a solution to minimize battery replacement cost by developing self-powered wireless sensors. Among ambient energy sources, vibration energy can be converted into electrical energy using a piezoelectric energy harvester that can generate an electrical alternating current in response to mechanical strain [1].

Especially, an analytical model for piezoelectric energy harvesting is of great importance to understand the first principle of energy conversion. Many researchers have developed analytical models of the piezoelectric energy harvester to predict harvestable electric power under a given vibration condition. However, there are still some challenges in this area. First, many analytical models, developed under deterministic excitation, cannot deal with random nature in realistic vibration signals, although the randomness considerably affects variation in harvestable electrical energy. Therefore, piezoelectric energy harvesting under the non-stationary random vibration should be analyzed in a stochastic manner. Second, there is no analytical model of an energy harvesting skin (EH skin) which is an innovative design for a piezoelectric energy harvester plate. Therefore, it is necessary to develop the analytical model of the EH skin. To successfully utilize

the self-powered wireless sensors by piezoelectric energy harvesting, these two practical issues on the analytical model are worked out in this thesis.

1.2 Overview and Significance

This research aims at advancing two essential and co-related research areas to develop the analytical model for piezoelectric energy harvesting: 1) Research Thrust 1 - stochastic electric power prediction under non-stationary random vibrations, 2) Research Thrust 2 - electromechanically coupled analytical model of the EH skin. To properly address these key research issues, the research scope in this thesis is to develop technical advances in the following two research thrusts:

Research Thrust 1: Stochastic Electric Power Prediction under Non-Stationary Random Vibrations

Research Thrust 1 proposes the three-step framework for the stochastic analysis of piezoelectric energy harvesting under non-stationary random vibrations consists of three sequentially executed procedures: (1) to estimate the time-varying PSD of input non-stationary random vibration signal using a time-frequency analysis, (2) to employ an electromechanical system as a linear operator, and (3) to estimate the time-varying PSD of output voltage response. Specific techniques and guidelines are also explained for each step.

Research Thrust 2: Electromechanically Coupled Analytical Model of the EH Skin

Research Thrust 2 develops the analytical model of the EH skin based on the Kirchhoff plate theory. In addition, analytical study of electromechanical behavior of the EH skin is performed from two different perspectives: (1) electric power estimation and (2) extraction of inflection lines. First, electric power in the resonance and anti-resonance frequency case is respectively predicted under a given vibration condition. In addition, inflection lines are designed for piezoelectric material segmentation to avoid the voltage cancellation under a given boundary condition.

1.3 Thesis Layout

This thesis is organized as follows: Chapter 2 reviews essential issues on piezoelectricity, design paradigm, and analytical models of the piezoelectric energy harvesting. Chapter 3 presents the three-step framework of the stochastic piezoelectric energy harvesting analysis under non-stationary random vibrations. Chapter 4 presents the electromechanically coupled analytical model of the EH skin using the plate theory. Finally, Chapter 5 summarizes the contributions of the research works and gives insights on future works.

Chapter 2. Literature Review

In this chapter, the state-of-art knowledge for piezoelectric energy harvesting within the scope of this thesis will be reviewed: (1) essential issues on piezoelectricity, (2) research topics of piezoelectric energy harvesting, and (3) analytical models of the piezoelectric energy harvester.

2.1 Piezoelectricity

2.1.1 Piezoelectric Effect

The prefix piezo comes from the Greek piezein which means to pressure or squeeze. Electricity is a physical phenomenon related to the flow of the electric charge. Therefore, piezoelectricity is "an interaction between electrical and mechanical behavior" [2].

As direct piezoelectric effect, a piezoelectric material can produce electrical energy (electric polarization) due to applied mechanical strain. Piezoelectric energy harvesting and piezoelectric transducers correspond to the direct piezoelectric effect. The amount of voltage generation is proportional to dynamic strain, as shown in Figure 2-1. Conversely, when the electric polarization is applied, the piezoelectric material becomes strained. This is called the inverse piezoelectric effect and piezoelectric actuators are typical example.

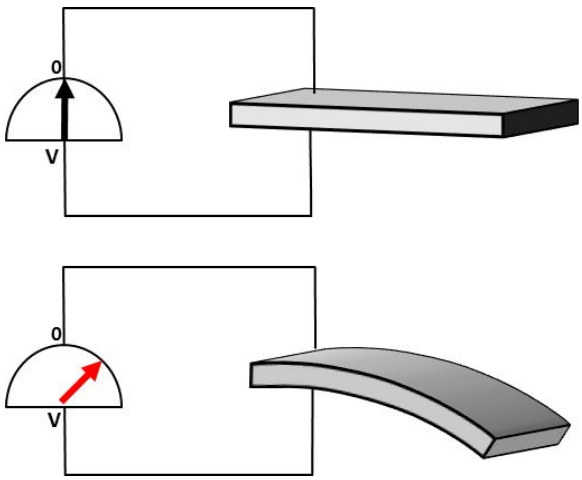

Figure 2-1 Direct Piezoelectric Effect of Piezoelectric Materials

2.1.2 Constitutive Relations

In IEEE Standard on Piezoelectricity (1987), the piezoelectric constitutive relations are given as [3]

$$T_{ij} = c_{ijkl}^{E} S_{kl} - e_{kij} E_k \tag{2.1}$$

$$D_i = e_{ikl} S_{kl} - \varepsilon_{ij}^{S} E_k \tag{2.2}$$

These expressions are also called the stress-charge form. In this case, the independent variables are strain S_{kl} and electric field E_k. It is noted that elastic constant c_{ijkl}^{E} and relative permittivity ε_{ij}^{S} (also called dielectric constant) are coupled to each other [4].

To calculate the electric current $i(t)$ in response to applied mechanical strain, Gauss's law, also known as Gauss's flux theorem, can be used with respect to the electric displacement D_i in an integral form as [5]

$$i(t) = \frac{d}{dt}\left(\Phi_D\right) = \frac{d}{dt}\left(\int_A \boldsymbol{D} \cdot \boldsymbol{n} dA\right) \tag{2.3}$$

where Φ_D is the electric displacement flux related to free charge. Because the unit vector $\boldsymbol{n}$ refers to the outward normal vector of the surface of the piezoelectric material, the direction of ($\boldsymbol{D} \cdot \boldsymbol{n}$) is determined in accordance with the poling direction.

2.2 Piezoelectric Energy Harvesting

Energy harvesting which scavenges electric power from ambient energy sources has been explored to develop self-powered wireless sensors and possibly eliminate battery replacement cost for wireless sensors. Vibration energy is one of the widely available ambient energy sources and can be converted into electrical energy using piezoelectric [6, 7], electromagnetic [8, 9], electrostatic [10, 11], and magnetostrictive [12-14] transduction mechanisms. Among them, the piezoelectric energy harvesting has gained much attention due to high energy.

Piezoelectric energy harvesting requires multidisciplinary research such as mechanical engineering, material science, and electrical engineering. As a result, extensive but different research efforts have been exercised to enhance electric power generation in a variety of areas, as shown in Figure 2-2. Therefore, this section gives a brief review of the piezoelectric energy harvesting by classifying it into four categories: 1) piezoelectric energy harvester design, 2) piezoelectric materials, 3) circuit configuration, and 4) system integration. Specially, analytical models for piezoelectric energy harvesting analysis will be reviewed in Section 2.3.

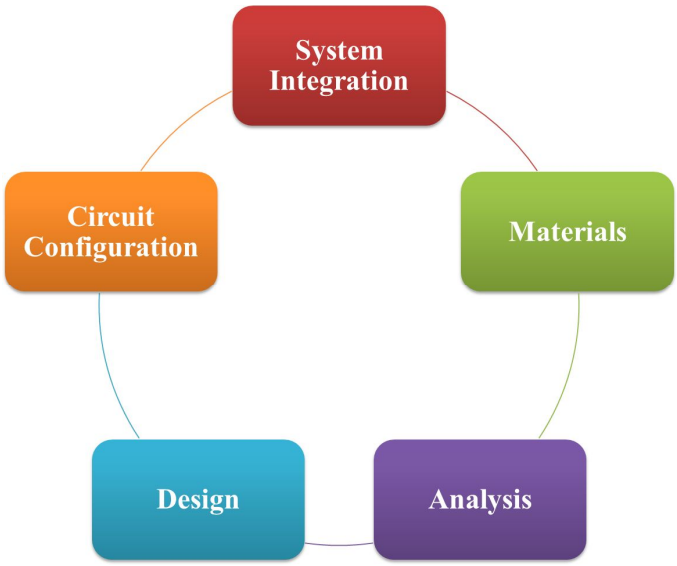

Figure 2-2 Research Topics of Piezoelectric Energy Harvesting

2.2.1 Piezoelectric Energy Harvester Design

From a mechanical point of view, the design challenges for the piezoelectric energy harvester follows as: 1) energy conversion efficiency, 2) random nature of realistic ambient vibrations, 3) wideband vibration, and 4) manufacturability. In the last decade, many design paradigms have been presented for reliably scavenging electrical energy to operate low-power electronics.

Cantilever Piezoelectric Energy Harvester

The piezoelectric energy harvester is typically designed as a cantilever beam with a single piezoelectric layer (unimorph) or two piezoelectric layers (bimorh) configurations. In general, the cantilever-type piezoelectric energy harvester is utilized as 31-mode that the directions of applied bending strain and generated

voltage are perpendicular to each other. Because the cantilever-type piezoelectric energy harvester achieves high mechanical strain and low natural frequency, they can produce relatively high electric power.

Roundy et al. (2005) investigated the design considerations to obtain high power output with the dimensions of the tip mass, the length, the thickness of the cantilever piezoelectric energy harvester, and optimal electrical load [15]. M. Kim et al. (2011) investigated mechanical behavior of a micro-scale piezoelectric energy harvester and the effect of the flexible tip mass and different electrode configurations [16]. Some researchers have investigated that a trapezoidal shape is more efficient than a rectangular shape because mechanical strain is uniformly distributed at every point along the beam length [17].

Energy Harvesting Skin (EH Skin)

Even though most piezoelectric energy harvesters are cantilever-type, they have some drawbacks: 1) additional space is required due to proof mass and clamping part, 2) a great deal of vibration energy can be lost when clamping conditions become loosened after long time use. These practical disadvantages can be overcome by the multifunctional EH skin, proposed by S. Lee and B. D. Youn (2011) [18]. The EH skin can be directly attached on the surface of vibrating mechanical systems, as shown in Figure 2-3.

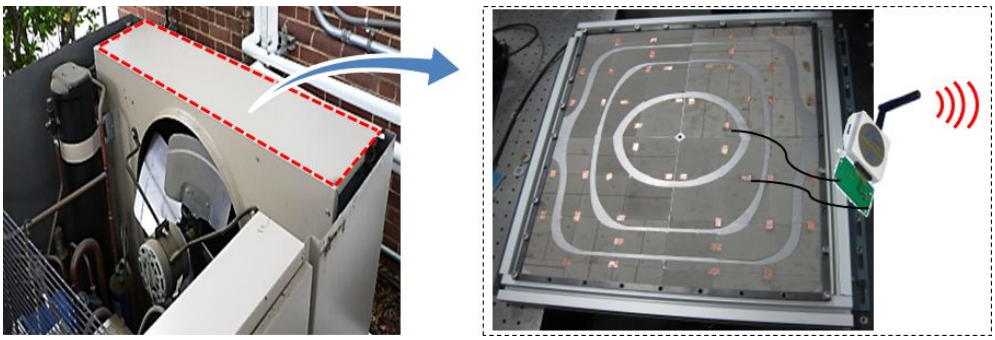

Figure 2-3 Concept of the Energy Harvesting Skin (EH Skin)

Resonant Frequency Tuning Scheme

When the resonance frequency of the piezoelectric energy harvester matches the dominant excitation frequency of ambient vibrations, electric power is maximized. Therefore, one of the most important design considerations is the resonant frequency matching. As a traditional approach, the resonant frequency of the piezoelectric energy harvester can be adjusted by changing its tip mass or stiffness. However, the excitation frequency and acceleration amplitude of realistic vibrations can vary as an operation condition (e.g., load and speed) of a machine. Recently, many adaptive resonant frequency tuning schemes have been proposed to overcome the dramatic reduction of electric power generation due to the variation of excitation frequency.

M. Lallart et al. (2010) proposed frequency self-tuning technique by using an additional actuator and excitation frequency detecting sensor [19]. S. Qi et al. (2010) proposed a multi-resonant beam for broadband piezoelectric energy harvesting which consists of multiple cantilever structures [20]. W. Al-Ashtari et al. (2012) presented frequency tuning scheme which can be accomplished by changing

the attraction force between two permanent magnets by adjusting the distance between the magnets [21].

2.2.2 Piezoelectric Materials

Because a PZT (Lead Zirconate Titanate), one of the most commonly available ceramics for piezoelectric energy harvesting, is electromechanically efficient and has a high piezoelectric and dielectric constant, they can achieve much higher electric power than other piezoelectric materials. However, the PZT is inherently brittle and less durable. Meanwhile, a piezoelectric polymer, such as a PVDF (Polyvinylidene Fluoride), has high flexibility but low electromechanical coupling. Therefore, the development of new piezoelectric materials works towards improving the mechanical and electrical performance simultaneously.

X. Chen et al. (2010) developed a piezoelectric nanogenerator based on PZT nanofibers [22]. Y. Qi et al. (2010) transferred crystalline piezoelectric nano-scale ribbons of lead zirconate titanate from host substrates onto flexible rubbers [23]. Y. Qi et al. (2011) presented a novel strategy for overcoming the limitations of existing piezoelectric materials by generating wavy piezoelectric ribbons on silicone rubber [24]. J. H. Kim et al. (2009) proposed an eco-friendly piezoelectric energy harvester using the cellulose based electro-active paper (EAPap) [25].

2.2.3 Circuit Configuration

In addition to high efficient piezoelectric materials and design optimization of the piezoelectric energy harvester, an electrical circuit configuration is also required to maximize the electric power output. The circuit configuration generally consists of three stages: 1) energy capture, 2) energy rectification, and 3) energy storage, as

shown in Figure 2-4. One of the most important aspects in circuit configurations is the impedance matching between the piezoelectric energy harvester and the electrical regulation. Moreover, because the piezoelectric energy harvester produces alternating current in accordance with the sign change of curvature of dynamic strain, it is required to use an AC/DC converter to operate electronic devices.

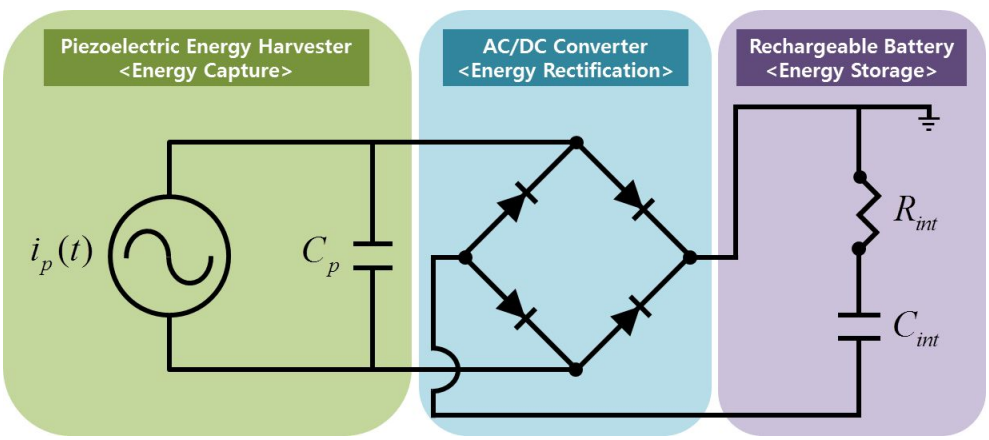

Figure 2-4 Circuit Configuration for Piezoelectric Energy Harvesting

There are many studies on the circuit conditioning. Ottman et al. (2003) studied an adaptive step-down DC–DC converter to maximize electric power from the piezoelectric energy harvester [26]. M. J. Guan et al. (2007) studied the efficiencies of the circuit configurations by comparing different storage device voltages [27].

2.2.4 System Integration

We are sometimes faced with a practical question whether piezoelectric energy harvesting makes it feasible to power real applications, such as low-power electronics, wireless sensors, etc. To successfully utilize self-powered electronics

using piezoelectric energy harvesting, we need to integrate the aforementioned research areas. S. Lee and B. D. Youn (2011) demonstrated that the EH skin can scavenge electric power from the vibration energy of a condensing unit in an outdoor air conditioner [28]. According to the experimental demonstration, electric power of 3.7 mW was obtained which is enough for operating wireless sensors. S. W. Arms et al. (2005) demonstrated smart wireless sensing nodes using piezoelectric energy harvesting [29].

2.3 Analytical Models for Piezoelectric Energy Harvesting

Many researchers have developed analytical models for the piezoelectric energy harvesting for a conceptual design of the piezoelectric energy harvester [15], electric power prediction under a given vibration condition [30-34], and physical insight of the electromechanical behavior [35], as shown in Figure 2-5.

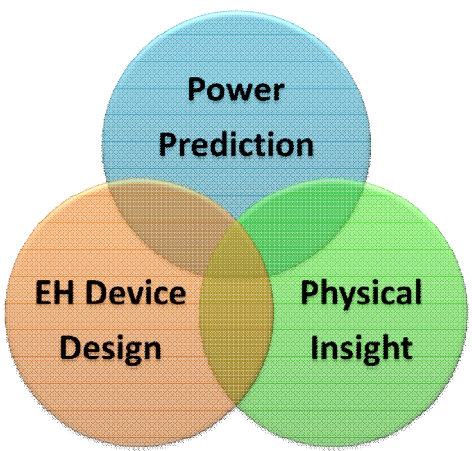

Figure 2-5 Functions of the Analytical Model of the Piezoelectric Energy Harvesting

Because the objective of this thesis is to develop the analytical model in a two-fold sense as 1) stochastic electric power prediction and 2) plate theory based analytical model of the EH skin, literatures on the analytical models are intensively discussed in this section and a summary is presented at the end.

2.3.1 Deterministic Approach for Harmonic Excitation

In the deterministic approach, the input excitation is assumed to be harmonic sinusoidal function. S. Round et al. (2004) developed a single degree of freedom lumped-parameter model for cantilever beam but there is no physical information, such as a dynamic strain distribution [30]. H. A. Sodano et al. (2005) formulated a single degree of freedom model and studied electric charge performance [31]. Because the lumped-parameter model might yield highly inaccurate results, A. Erturk et al. (2008) developed an amplitude correction factor with tip-mass to beam mass ratio to accurately predict the voltage response of the lumped-parameter model [32]. N. E. DuToit et al. (2007) derived an approximate distributed-parameter model using the Rayleigh-Ritz discretization [33]. A. Erturk et al. (2009) proposed the exact solution of electromechanically coupled distributed-parameter model for cantilever mean and compared it to experimental observations [34].

2.3.2 Stochastic Approach for Random Excitation

In practice, however, most excitations are broadband random vibrations. There have been several attempts to develop the analytical model under random vibrations. It is assumed in most existing stochastic models that the excitation form be a white Gaussian noise which is wideband and has a constant power spectral density (PSD).

E. Holvorsen (2008) formulated stochastic description using the PSD for electric

power, proof mass displacement, and optimal load of resonant energy harvesters based on Fokker-Plank equation [36]. S. Adhikari et al. (2009) presented closed-form of a linear SDOF model when excitation is assumed as a white Gaussian noise with a flat PSD [37]. T. Seuaciuc-Osorio et al. (2010) investigated harvestable energy subjected to a harmonic excitation of a sinusoidally varying frequency case with fixed amplitude [38]. S. F. Ali et al. (2011) developed an equivalent linear model for piezomagnetoelastic energy harvesters under broadband random vibration [39]. S. Zhao et al. (2013) predicted expected electric power and the mean-square shunted displacement based on the PSD by employing the Fourier series representation or an Euler-Maruyama scheme to solve the stochastic differential equations [40].

2.3.3 Plate Theory Based Analytical Models

The analytical models, based on a beam theory, can be limitedly applicable to cantilever piezoelectric energy harvesters which have a large length-to-width ratio. Analytical models of piezoelectric plates for active damping, dynamic absorber, and actuation have been considerably developed so far. Although many computational approaches have been developed for the analysis of the electromechanical behavior and the topology optimization of the piezoelectric energy harvester [41, 42], only a few analytical models based on plate theory have been covered in piezoelectric energy harvesting.

S. Kim et al. (2005) calculated electric power with varying thickness ratios using the clamped unimorph circular plate model and investigated the effect of the electrodes on net charge generation [43]. A. Erturk (2011) derived an analytical plate model for electric power prediction from dynamic strain components

measured by strain gage rosettes [44]. S. Yu et al. (2012) presented a free vibration analysis for a laminated piezoelectric cantilever plate [45] using the superposition method, developed by Gorman (1976) [46].

2.3.4 Summary and Discussion

Although the analytical models, aforementioned in Section 2.3.2, have been developed for random vibrations (stationary white Gaussian noise), they cannot be implemented when the statistical moments of acceleration signals (e.g., mean value, autocorrelation function, and power spectral density) randomly change with time. Therefore, the three-step framework of the stochastic piezoelectric energy harvesting analysis under non-stationary random vibrations is proposed in research thrust 1. Specially, a statistical time-frequency analysis is first applied to deal with random nature of realistic vibration signals.

Furthermore, although there have been plate based analytical model for cantilever plate with a moderate aspect ratio, there is no analytical model of the EH skin. Therefore, the electromechanically coupled analytical model of the EH skin using a plate theory is theoretically investigated in research thrust 2.

Chapter 3. Stochastic Electric Power Prediction under Non-stationary Random Vibrations

The predictive capability of an analytical models is normally poor under random vibrations. Such a poor electric power prediction is mainly caused by the variation of the excitation frequencies and their peak acceleration levels. Therefore, stochastic electric power prediction should be able to systematically handle the random nature in realistic vibration signals of engineered systems. To address this challenge, Chapter 3 is organized as follows: Section 3.1 gives an overview of stochastic piezoelectric energy harvesting analysis proposed in this study. Section 3.2 explains how to model the non-stationary random vibration signal. Section 3.3 presents a statistical time-frequency analysis to estimate the time-varying PSD of an input non-stationary random vibration. An electromechanical system as the linear operator for calculating the output voltage response is explained in Section 3.4. Finally, Section 3.5 explains how to estimate the time-varying PSD of output voltage response.

3.1 Overview of Stochastic Piezoelectric Energy Harvesting Analysis

3.1.1 Fundamentals of Non-Stationary Random Vibrations

Stochastic Process

A stochastic process refers to "a family of random variables" [47]. At this

moment, a non-stationary random vibration signal can be considered as a one-dimensional stochastic process. The possibility to mathematically deal with random nature depends on whether the stochastic process has a statistical pattern. If so, the stochastic process can be described in terms of statistical moments or probability density function to extract meaningful information of the signal. If the stochastic process is stationary, ensemble averages which computes statistical moments over the entire collection of signals can be replaced by time averages which calculate statistical moments using only one representative signal over time. In this case, the stochastic process is said to be an ergodic process.

Autocorrelation Function

The autocorrelation function of $x(t)$ is "a measure that the degree of association of the signal at time $(t - \tau/2)$ with itself at time $(t + \tau/2)$" [47]. It is defined as

$$R_X(t,\tau) = E\left[x\left(t + \frac{\tau}{2} \right) x^*\left(t - \frac{\tau}{2} \right) \right] \tag{3.1}$$

Another definition is the inverse Fourier transform of the time-varying PSD.

Time-Varying Power Spectral Density

When the random vibration signal is non-stationary, the stochastic process, described in frequency domain using the PSD, also depends on time t as

$$S_X(t,\omega) = \int_{-\infty}^{\infty} R_X(t,\tau) e^{-i\omega\tau} d\tau \tag{3.2}$$

The physical meaning of the time-varying PSD is that the local average power of the variance is decomposed in the time and frequency domains.

3.1.2 Framework of Stochastic Piezoelectric Energy Harvesting Analysis under Non-Stationary Random Vibrations

Based on Section 3.1.1, this section discusses the framework of stochastic piezoelectric energy harvesting analysis under non-stationary random vibration. The proposed framework consists of three sequentially executed procedures, as shown in Figure 3-1.

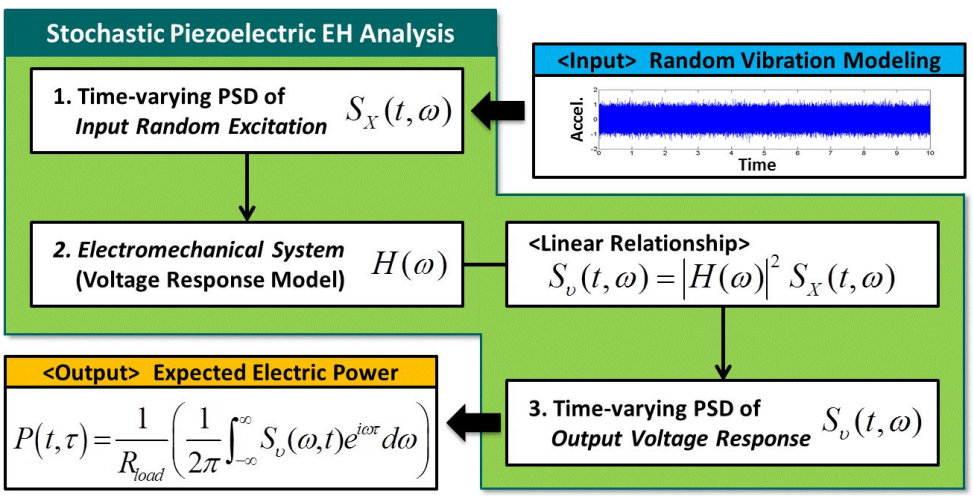

Figure 3-1 Framework of Stochastic Piezoelectric Energy Harvesting Analysis

Time-Varying PSD Estimation of Input Non-Stationary Random Vibrations

The first step is to estimate the time-varying PSD of input non-stationary random vibrations, denoted by $S_X(\omega)$. There are two main tasks in the first step: (1) modeling of non-stationary random vibration signal and (2) statistical time-frequency analysis to estimate time-varying PSD.

Electromechanical System Employment

The second step is to employ an electromechanical system as a linear operator. In the proposed framework of the stochastic piezoelectric energy harvesting analysis, the linear operator, denoted by $H(\omega)$, implies the linear relationship between the time-varying PSD of the random vibration and the time-varying PSD of the voltage response.

Time-Varying PSD Estimation of Output Voltage Response

The third step is to estimate the time-varying PSD of the output voltage response, denoted by $S_v(\omega)$, from the linear relationship. In a stochastic approach, the expected electric power can be obtained from the autocorrelation function that is inverse Fourier transform of the time-varying PSD of the output voltage response.

3.2 Modeling of the Non-Stationary Random Vibration Signal

In most cases, "inherent nonlinearity of vibrating systems, load fluctuation, and operating speed affect the statistics of the measured vibration signals over time" [48]. It implies that most realistic vibration signals of engineered systems are usually non-stationary. Then, vibration analysis focuses on "the extraction of physically meaningful information from the mathematical representation" based upon a single vibration signal realization [49, 50]. In the proposed framework of the stochastic piezoelectric energy harvesting analysis, the non-stationary random vibration signal $x(t)$ was modeled with a multiplicative noise as [51]

$$x(t) = m(t) \cdot \sin\left[\alpha \cdot \{\varepsilon(t) \cdot \omega\} \cdot t\right] \tag{3.3}$$

$$m(t) = \sum_{k=1}^{p} c_k(t) \cdot m(t-k) + \sigma(t) \tag{3.4}$$

where $m(t)$ is an autoregressive function, $\varepsilon(t)$ and $\sigma(t)$ are frequency and amplitude modulation parameters that are modeled with a white Gaussian noise. Figure 3-2 shows the non-stationary random vibration signal.

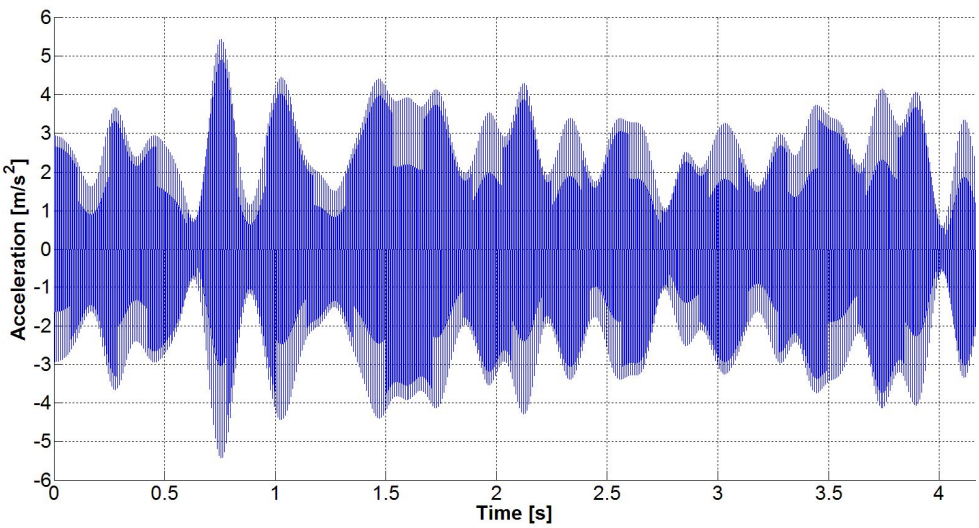

Figure 3-2 Random Vibration Signal modulated by Multiplicative Noise

Although the mean value of the vibration signal is zero-constant, the root mean square level is time-varying. For this non-stationary random signal, the traditional PSD does not exist in the frequency domain. Therefore, a time-frequency analysis is needed to estimate the time-varying PSD of non-stationary random vibrations.

3.3 Time-varying Power Spectral Density of the Non-stationary Random Vibration

This section explains how to estimate the time-varying PSD of the input non-stationary random vibration signal using a time-frequency analysis. The vibration signal can be localized in both time and frequency domains. The time localization means to specify the signal appeared during a time interval. On the other hand, the frequency localization identifies the signal components which are concentrated at particular Fourier spectrum [52]. Therefore, the selection of the time-frequency representation plays an important role for correctly extracting probabilistic information of the vibration signal. In this study, the Wigner-Ville spectrum was used to estimate the time-varying PSD of a non-stationary random vibration signal modulated by a multiplicative noise.

3.3.1 Wigner-Ville Spectrum

For the localization of the signal modulated by a multiplicative noise, the Wigner-Ville distribution (WVD) is optimal to estimate the energy distribution in both frequency and time domains. It is defined as

$$WVD_X(t,\omega) = \int_{-\infty}^{+\infty} x\left(t-\frac{\tau}{2}\right)x^*\left(t+\frac{\tau}{2}\right)e^{-i\omega\tau}d\tau \tag{3.5}$$

The Wigner-Ville distribution is one of the most commonly used time-frequency analyses and there is an analogy with a probability density function (PDF) [52]. The time-varying PSD $S_X(t,\omega)$ is defined as the Fourier transform of the autocorrelation function $R_X(t,\tau)$ which form is similar with the Wigner-Ville distribution. Therefore, the time-varying PSD can be obtained by the ensemble

average of the Wigner-Ville distribution [53], so called Wigner-Ville spectrum as

$$\begin{aligned} S_X(t,\omega) &= \int_{-\infty}^{\infty} R_X(t,\tau) e^{-i\omega\tau} d\tau \\ &= \int_{-\infty}^{\infty} E\left[x\left(t+\frac{\tau}{2}\right) x^*\left(t-\frac{\tau}{2}\right)\right] e^{-i\omega\tau} d\tau \\ &= E\left[\int_{-\infty}^{\infty} x\left(t+\frac{\tau}{2}\right) x^*\left(t-\frac{\tau}{2}\right) e^{-i\omega\tau} d\tau \right] \\ &= E\left[WVD_X(t,\omega)\right] \end{aligned} \tag{3.6}$$

However, it is extremely difficult to directly use the Wigner-Ville spectrum because this ensemble average expression demands a great deal of the signal realizations. Alternatively, it is possible to calculate statistical moments by averaging only one representative signal over time, according to an ergodic process. As a result, it is assumed that the Wigner-Ville distribution be locally ergodic in a smoothing kernel function so as to replace the ensemble averages by time averages [53]. By taking the time averages of the Wigner-Ville distribution, we can estimate the time-varying PSD which is the Wigner-Ville spectrum of the non-stationary random vibration with the multiplicative noise signal as

$$\hat{S}_X(t,\omega) = \int\int_{-\infty}^{+\infty} W_x(u,v)\Pi(t-u,\omega-v) du dv \tag{3.7}$$

This expression is the same with the unified framework of Cohen's class, denoted by $C_X(t,\omega;\Pi)$ [54]. It can be also considered as two-dimensional convolution. There are two famous Wigner-Ville spectrum estimators, the spectrogram and the smoothed pseudo Wigner-Ville distribution which are the most widely used. Before implementing the Wigner-Ville spectrum estimator, a suitable smoothing window should be first chosen.

3.3.2 Smoothing Window Choice

The resolvability depends on the choice of the smoothing kernel functions used in the Wigner-Ville spectrum. Therefore, the appropriate shape and size of the window should be carefully selected for the optimal localization. In general, a Rectangular, Gauss, Hamming, Hanning, and Kaiser windows are used in different vibration signals through a compromise between the smearing due to the main lobe and the leakage due to the side lobes caused by the convolution operation in the smoothing window [47].

NATIONAL INSTRUMENTS (NI) Corp. offers the strategies for selecting a kernel function based on its own characteristics as follows [55]: For example, to resolve several closely spaced frequency components in the signal, a smoothing window with a narrow main lobe is suitable. Meanwhile, if the amplitude is more significant than the location of a frequency component, a smoothing window with a wide main lobe is recommended. On the other hand, if the random vibration signal contains interference terms (or cross-terms), natural characteristic of a bilinear representation (e.g., the Wigner-Ville spectrum), are far from the frequency of interest, a smoothing window with a high side lobe roll-off rate is recommended. In contrast, if interference terms exist near the frequency of interest, a smoothing window with a low highest side lobe is a good candidate.

In general, “the Hanning window with a moderate frequency resolution and a good side lobe roll-off” is acceptable in most cases [48]. Furthermore, the Hanning window is suitable for spectral analysis of random vibrations or noise measurements. The Flat top window is usually used when the accuracy of the sinusoidal wave amplitude is important. In this study, therefore, the Hanning window was used for the time and frequency smoothing in the spectrogram. On the

other hand, the Flat top and the Hanning window were respectively used for the time smoothing and the frequency smoothing in the smoothed pseudo Wigner-Ville distribution.

3.3.3 Wigner-Ville Spectrum 1: Spectrogram

The definition of the spectrogram is given as

$$\hat{S}^{g}_{Spg}(t,\omega) = \int_{-\infty}^{+\infty}\int_{-\infty}^{+\infty} W_x(\tau,v) W_g(\tau - t, v - \omega)\, d\tau\, dv \tag{3.8}$$

The spectrogram of the multiplicative noise is shown in Figure 3-3.

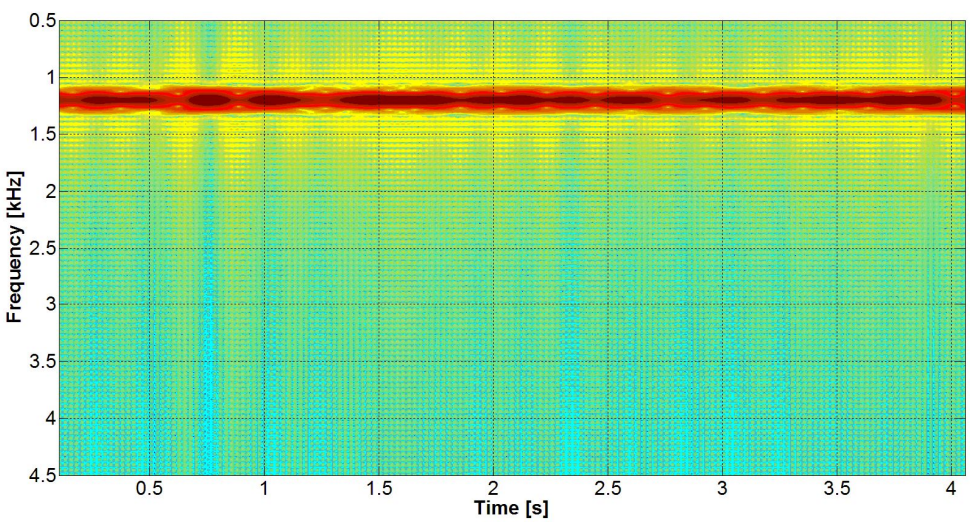

Figure 3-3 Spectrogram of the Multiplicative Noise

As shown in Figure 3-3, since the one smoothing window $W_g(\tau-t,v-\omega)$ is used in both time and frequency domains, the frequency was smeared according to the

Heisenberg-Gabor uncertainty principle which leads to a trade-off between time and frequency resolution [52]. In other words, the resolution cannot be improved in both the time and frequency domains simultaneously. For example, "the shorter the duration of time window, the better time resolution, but the larger the bandwidth of the spectrum, and the poorer frequency resolution" [56].

3.3.4 Wigner-Ville Spectrum 2: Smoothed Pseudo Wigner-Ville Distribution (SPWVD)

On the other hand, the smoothed pseudo Wigner-Ville distribution adjusts the time and frequency smoothing kernel function separately as

$$\hat{S}_{SPWV}^{g,h}(t,\omega)=\int_{-\infty}^{+\infty}\int_{-\infty}^{+\infty}W_x(\tau,v)g(\tau-t)H(v-\omega)d\tau dv \tag{3.9}$$

The use of separable kernel functions allows the control of the smoothing performance in time and frequency domain respectively [52]. In this study, the sizes of the Hanning window and the Flat top window were 5 points in time and 251 points in frequency respectively. As we expect, the readability of the smoothed pseudo Wigner-Ville distribution is better than that of the spectrogram. The high amplitude of the signal is represented as red in the time-varying PSD, as shown in Figure 3-4.

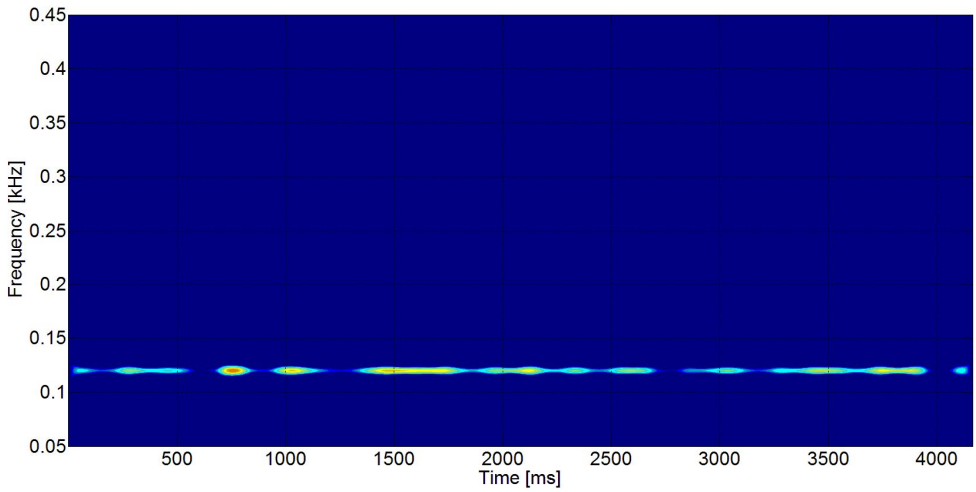

Figure 3-4 Smoothed Pseudo Wigner-Ville Distribution of the Multiplicative Noise

Finally, in this study, the smoothed pseudo Wigner-Ville distribution is selected as the estimator for the time-varying PSD of the input non-stationary random vibration signal modulated by the multiplicative noise.

Reassigned Smoothed Pseudo Wigner-Ville Distribution

If the non-stationary random vibration signal is a multi-component frequency modulation (FM), the smearing problem is more serious due to inherent characteristic of smoothing kernel functions. For improving the localization, "the reassignment technique which consists of a smoothing to reduce interferences and a squeezing to refocus components" can be used [56]. This technique rearranges the values of the Wigner-Ville distribution "not to the center of geometry but the center of mass in the smoothing window" by computing a centroid point as [56-57]

$$\hat{t}_x(t,\omega) = t - \frac{\hat{S}^{tg,h}_{X,SPWV}(t,\omega)}{\hat{S}^{g,h}_{X,SPWV}(t,\omega)} \tag{3.10}$$

$$\hat{\omega}_x(t,\omega) = \omega + i\frac{\hat{S}^{g,dh/dt}_{X,SPWV}(t,\omega)}{\hat{S}^{g,h}_{X,SPWV}(t,\omega)} \tag{3.11}$$

3.4 Electromechanical System as the Linear Operator

One of the most important things in stochastic process is "to find the linear operator and make it possible for analytical implementation to get certain probabilistic information" [58]. As long as an existing electromechanically-coupled analytical model can be expressed by a frequency response function (FRF) between the output voltage and the input acceleration level at arbitrary excitation frequency ω, it can be employed as the linear operator.

In this study, the distributed-parameter electromechanical model for a bimorph cantilever piezoelectric energy harvester, established by Erturk and Inman [33], was employed. This Section briefly introduces its derivation procedure and explains the physical interpretation of each expression.

3.4.1 Mechanical Equation of Motion and Modal Analysis

The cantilever piezoelectric energy harvester is utilized as 31-mode bimorph configuration that the direction of applied stress and generated voltage are perpendicular to each other. It can be modeled as thin Euler-Bernoulli beam which neglects the effects of rotary inertia and shear deformation [59]. In this case, the damped mechanical equation of motion is expressed by a fourth-order partial differential equation with two boundary conditions. For the boundary conditions,

fixed at $x = 0$ and free at $x = l$, the transverse deflection and its slope is zero at $x = 0$ and the bending moment and shear force is zero at $x = l$. As a result, the characteristic equation is given as

$$\cos(\lambda_n)\cdot\cosh(\lambda_n)+1=0 \tag{3.12}$$

The nth mode shape can be expressed as [59]

$$\begin{aligned}&\psi_n(x)\\&=\left[\cos(\beta_n x)-\cosh(\beta_n x)\right]-\frac{\cos(\beta_n L)+\cosh(\beta_n L)}{\sin(\beta_n L)+\sinh(\beta_n L)}\left[\sin(\beta_n x)-\sinh(\beta_n x)\right]\end{aligned} \tag{3.13}$$

The bending stiffness Y_sI of bimorph cantilever composite with three layers is as [34]

$$Y_sI=\frac{2b}{3}\left[Y_s\left(\frac{h_s^3}{8}\right)+c_{11}^E\left\{\left(h_p+\frac{h_s}{2}\right)^3-\frac{h_s^3}{8}\right\}\right] \tag{3.14}$$

The nth natural frequencies can be calculated as

$$\omega_n=\lambda_n^2\sqrt{\frac{Y_sI}{ml^4}} \tag{3.15}$$

Because the mode shapes from boundary value problem are orthogonal, it can be used to formulate an expansion theorem as [60].

$$w_{rel}(x,t)=\sum_{n=1}^{\infty}\psi_n(x)\eta(t) \tag{3.16}$$

In the Sturm-Liouville problem, the sets of the orthogonal mode shapes $\psi_n(x)$ are complete in $L_2(0, l)$ space, the relative displacement $w_{rel}(x,t)$ absolutely and uniformly converges in the series of mode shapes [61].

Therefore, the mechanical equation in modal coordinates can be expressed by as [34]

$$\frac{\partial^2 \eta(t)}{\partial t^2} + 2\zeta\omega_n \frac{\partial \eta(t)}{\partial t} + \omega_n{}^2 \mu(t) - \boldsymbol{\theta}_n \upsilon(t) = f(t) \tag{3.17}$$

where the electromechanical coupling, denoted by $\boldsymbol{\theta}_n$, is expressed as [34]

$$\boldsymbol{\theta}_n = \bar{e}_{31} \left(\frac{h_p + h_s}{2} \right) \frac{d\psi_n(x)}{dx}\bigg|_{x=l} \tag{3.18}$$

3.4.2 Electrical Circuit Equation

In an electrical domain, the electrical circuit equation was derived by integrating the electric displacement D_3 in the piezoelectric constitutive relation in Eq. (2.2) with the electrical current obtained from the Gauss's law in Eq. (2.3).

$$\begin{aligned} &\frac{\vartheta(t)}{R_{load}} \\ &= \frac{d}{dt}\left(\int_A D_3 dA \right) \\ &= \frac{d}{dt}\left\{ \int_A (\bar{e}_{31} S_1 + \varepsilon_{33}^S \mathrm{E}_3) dA \right\} \\ &= -\bar{e}_{31} b \left(\frac{h_p + h_s}{2} \right) \int_0^L \left\{ \frac{\partial^3 w_{rel}(x,t)}{\partial x^2 \partial t} \right\} dx - \frac{\varepsilon_{33}^S bL}{h_p} \left(\frac{d\vartheta(t)}{dt} \right) \end{aligned} \tag{3.19}$$

where dynamic strain component S_1 can be expressed as

$$S_1 = -h_{pc} \frac{\partial^2 w_{rel}(x,t)}{\partial x^2} \tag{3.20}$$

By substituting Eq. (3.16) and Eq. (3.18) into Eq. (3.19), the electrical circuit equation can be expressed in modal coordinates as [34]

$$C_p\dot{\upsilon}(t)+\frac{\upsilon(t)}{R_{load}}+\sum_{n=1}^{\infty}\theta_n\dot{\eta}(t)=0 \tag{3.21}$$

where C_p is a capacitance given as

$$C_p=\frac{\varepsilon_{33}^S bL}{h_p} \tag{3.22}$$

3.4.3 Steady-State Voltage Response

Finally, the steady-state voltage response can be obtained by solving the mechanical equation of motion and electrical circuit equation simultaneously as [34]

$$H(\omega)=\frac{j\omega R_{load}\theta}{\left(1+i\omega R_{load}\frac{C_p}{2}\right)\left(\omega_n^2-\omega^2+i2\zeta\omega_n\omega\right)+j\omega R_{load}\theta^2} \tag{3.23}$$

As the impedance matching for the maximum electric power, the optimal external load at the short-circuit resonance frequency can be obtained by setting as

$$\frac{\partial\left[\frac{H(\omega)^2}{R_{load}}\right]}{\partial R_{load}}=0 \tag{3.24}$$

In a result, the optimal external resistance is expressed as [62]

$$R_{load}^{opt,\omega_r^{sc}}=\frac{1}{\omega_r C_p\left[1+\left\{\frac{\overline{e}_{31}b\left(h_p+h_c\right)}{4\zeta_r^2}\left(\frac{d\psi_r(x)}{dx}\bigg|_{x=l}\right)\right\}^2\right]^{1/2}} \tag{3.25}$$

According to Eq. (3.25), the optimal external resistance only depends on mechanical (e.g., natural frequency, mode shape, geometry, damping ratio) and electrical (e.g., piezoelectric constant, capacitance) parameters of the piezoelectric energy harvester. It means that the optimal external resistance does not depend on the given vibration condition, if the excitation frequency of the vibrating structure is adjacent to resonance frequency. Therefore, the optimal external resistance, derived under the assumption of the deterministic excitation, can be also used under non-stationary random vibrations.

Finally, $H(\omega)$ was calculated using the material properties of T226-H4-503X from Piezo Systems, Inc., as shown in Table 1. The fundamental natural frequency was calculated as 119.11 Hz from Eq. (3.15) and the optimal external resistance at short-circuit resonance frequency was obtained as 4250 Ω.

Table 1 Mechanical and Electrical Parameters of Cantilever Beam Piezoelectric Energy Harvester

Mechanical Parameters		**Electrical Parameters**	
c_{11}^{E}	62 GPa	d_{31}	-3.20×10^{-10} m/V
Y_s	124 GPa	e_{31}	-19.84 C/m^2
h_p	0.2667 mm	ε_0	8.854 pF/m
h_s	0.1016 mm	ε_{33}^{T}	33.65 nF/m
ρ_p	7500 kg/m^3	ε_{33}^{S}	27.30 nF/m
ρ_s	7800 kg/m^3	C_p	82.78 nF
$1/(2\zeta)$	30	θ	6.91×10^{-3} N/m
l	51.5 mm	R_{load}	4250 Ω
b	31.8 mm		

3.5 Time-varying Power Spectral Density of the Voltage Response

3.5.1 Estimation of the Time-Varying PSD of the Output Voltage Response

The time-varying PSD of the output voltage response was estimated from the linear relationship between the input and output time-varying PSD. From a physical point of view, “if the input excitation is the stochastic process, the output response is also the stochastic process” [58]. As a stochastic dynamics, the linear relationship

is expressed as

$$S_{\upsilon}(\omega,t) = \left|H(\omega)\right|^2 S_X(\omega,t) \tag{3.26}$$

Figure 3-5 shows the time-varying PSD of the Output voltage response $S_{\upsilon}(t,\omega)$.

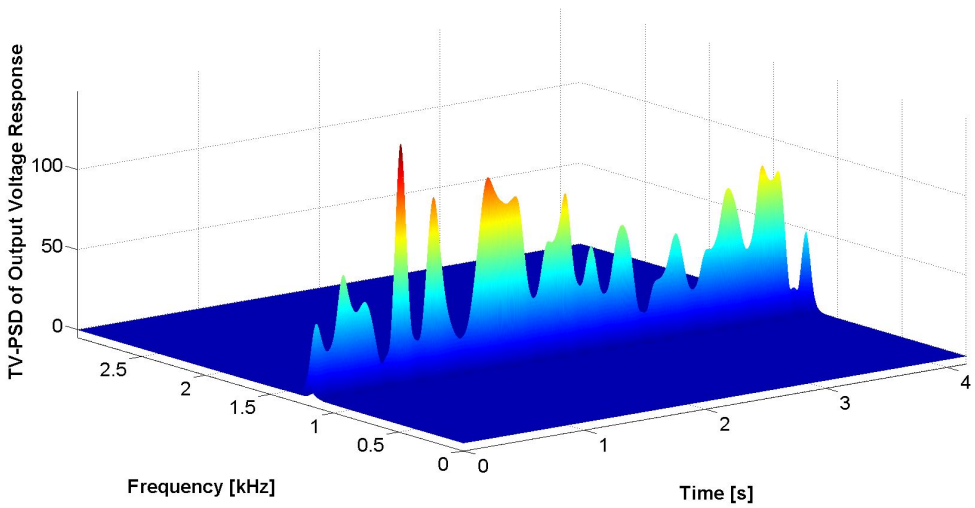

Figure 3-5 Time-Varying PSD of the Voltage Response

3.5.2 Expected Electric Power Prediction

As previously explained in Section 3.1, the autocorrelation function $R_{\upsilon}(t,\tau)$ can be obtained by the inverse Fourier transform of the time-varying PSD of the output voltage response as

$$R_{\upsilon}(t,\tau) = E\left[\upsilon\left(t-\frac{\tau}{2}\right)\upsilon\left(t+\frac{\tau}{2}\right)\right] = \frac{1}{2\pi}\int_{-\infty}^{\infty} S_{\upsilon}(\omega,t)e^{i\omega\tau}d\omega \tag{3.27}$$

Figure 3-6 shows the instantaneous autocorrelation function of the output voltage response.

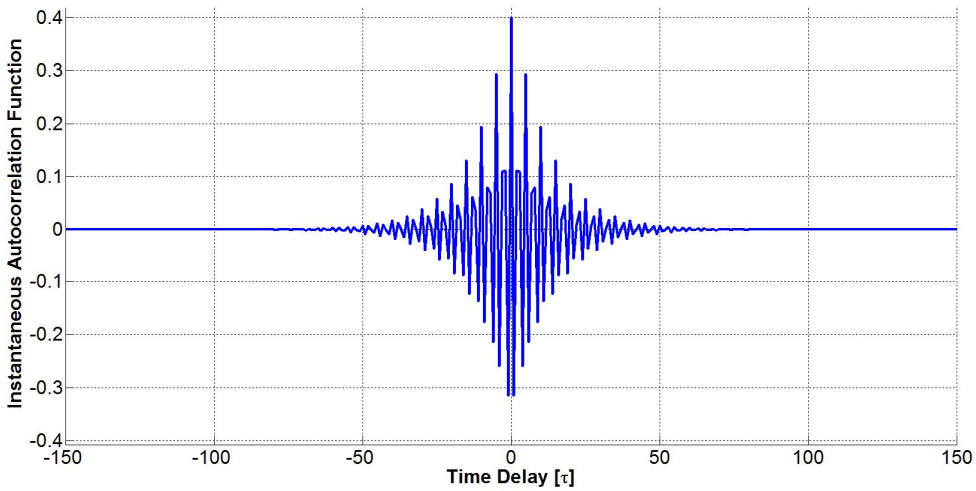

Figure 3-6 Instantaneous Autocorrelation Function of the Output Voltage Response

Finally, the expected electric power $P(t)$ can be obtained by taking zero time-lag ($\tau = 0$) as

$$E[P(t)] = \frac{E[\upsilon(t)^2]}{R_{load}} = \frac{1}{2\pi R_{load}} \int_{-\infty}^{\infty} S_{\upsilon}(\omega, t) e^{i\omega\tau} d\omega \Big|_{\tau=0} \tag{3.28}$$

Figure 3-7 is the real-time prediction result of the expected electric power. Because the electric power is proportional to square of acceleration, the phase of acceleration signal and that of expected electric power is exactly same. As shown in Figure 3-7, the maximum expected electric power is about 1173 μW with the maximum acceleration level of 5.305 m/s^2 at t = 0.753 s.

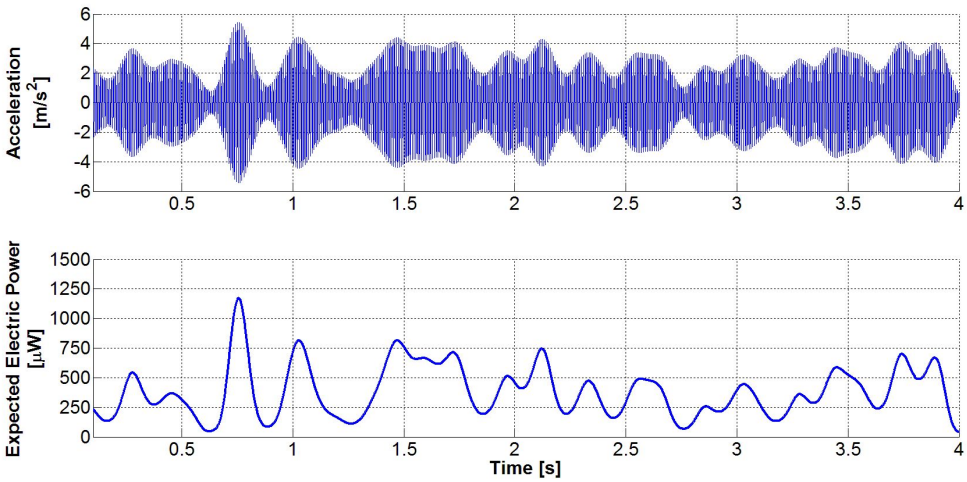

Figure 3-7 Expected Electric Power Prediction Result

Chapter 4. Plate Theory based Electromechanically Coupled Analytical Model of the EH Skin

In the past piezoelectric energy harvesters have primarily designed as a cantilever beam which requires a bulky device fixture. As an alternative design paradigm, the EH skin has been proposed to scavenge electric power from vibration energy of the engineered structure with an additional thin piezoelectric layer as one embodiment. This EH skin is also multifunctional since it enables noise reduction and load-carrying.

However, there is no analytical study of electromechanical behavior of the EH skin. This section discusses an electromechanically coupled analytical model of the EH skin. The plate theory based analytical model, developed in this study, is an extension of the electromechanically coupled distributed-parameter model for cantilever beam, proposed by A. Erturk (2009). Chapter 4 is organized as follows: Section 4.1 presents constitutive equations of the EH skin based on the Kirchhoff plate theory. In Section 4.2, the generalized Hamilton's principle is used to derive the governing differential equation of motion in a mechanical domain. Section 4.3 analyzed the natural frequencies and mode shapes of the EH skin are analyzed by the Levy's method. Section 4.4 derives the electrical circuit equation in an electrical domain. Section 4.6 predicts electric power under the vibration condition for different boundary cases. Finally, Section 4.7 gives a guideline to extract inflection lines of the EH skin for avoiding the voltage cancellation.

4.1 Constitutive Equations

4.1.1 Kirchhoff Plate Theory

Figure 4-1 shows the schematic view of the EH skin which consists of a piezoelectric layer and a substrate layer as the unimorph configuration. As explained in Section 2.2, the top surface of the substrate (e.g., brass, aluminum) is fully covered by the piezoelectric material.

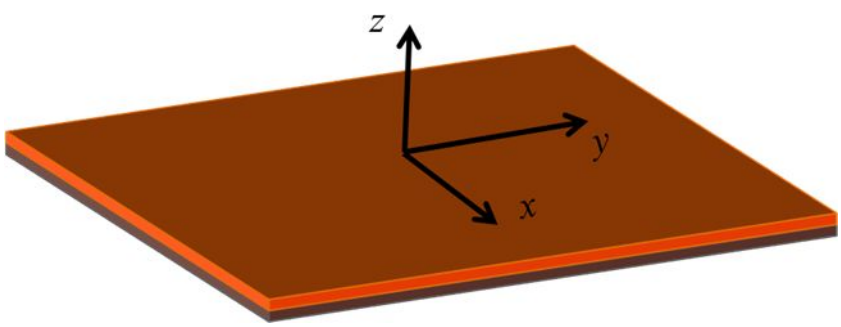

Figure 4-1 The Schematic View of the EH Skin

Furthermore, because the piezoelectric materials are generally manufactured as a thin plate, the EH skin can be modeled as the Kirchhoff plate which is analogue to the Euler-Bernoulli beam [63]. According to the Kirchhoff plate theory [64], the deflection of the middle surface is assumed to be small compared with the thickness of the EH skin. After bending, the middle surface remains unstrained as the neutral plane. In addition, the cross-sectional plane of the EH skin, initially normal to the middle surface, remain normal to that surface after bending. This means that the transverse shear strains γ_{xz} and γ_{yz} are negligible. Similarly, the normal strain ε_z under transverse vibration of the EH skin can be also omitted. Because the normal stress σ_z in the thickness direction is neglected under the assumption of the thin

plate, the state of stress in the EH skin is considered as a plane stress as

$$T_3 = T_4 = T_5 = 0 \tag{4.1}$$

Therefore, the constitutive equations of the substrate layer and piezoelectric layer are respectively reduced from Eq. (2.1) and Eq. (2.2) as

$$\begin{Bmatrix} T_1 \\ T_2 \\ T_6 \end{Bmatrix} = \frac{Y_s}{1-\nu_s^2} \begin{bmatrix} 1 & \nu_s & 0 \\ \nu_s & 1 & 0 \\ 0 & 0 & (1-\nu_s)/2 \end{bmatrix} \begin{Bmatrix} S_1 \\ S_2 \\ S_6 \end{Bmatrix} \tag{4.2}$$

$$\begin{Bmatrix} T_1 \\ T_2 \\ T_6 \\ D_3 \end{Bmatrix} = \begin{bmatrix} \overline{c}_{11}^E & \overline{c}_{12}^E & 0 & -\overline{e}_{31} \\ \overline{c}_{12}^E & \overline{c}_{11}^E & 0 & -\overline{e}_{31} \\ 0 & 0 & \overline{c}_{66}^E & 0 \\ \overline{e}_{31} & \overline{e}_{31} & 0 & \varepsilon_{33}^S \end{bmatrix} \begin{Bmatrix} S_1 \\ S_2 \\ S_6 \\ E_3 \end{Bmatrix} \tag{4.3}$$

4.1.2 Mechanical and Electrical Parameters

In general, piezoelectric ceramics have the same properties in the *x-y* plane and different properties in the z-axis, called transversely isotropic materials. That's why the constitutive equation in matrix form of piezoelectric ceramics is symmetry as

$$\overline{c}_{11}^E = \overline{c}_{22}^E \tag{4.4}$$

$$d_{31} = d_{32} \tag{4.5}$$

The poling direction of piezoelectric layer is the z-axis and it implies that the electric field is given as

$$E_1 = E_2 = 0 \tag{4.6}$$

$$E_3 = -\frac{\upsilon(t)}{h_p} \tag{4.7}$$

Because the only non-zero strains of the EH skin are in the *x*-*y* plane (in-plane directions), the direction of applied dynamic strain and generated voltage are perpendicular to each other. It means that the EH skin is utilized as the 31-mode.

In IEEE Standard on Piezoelectricity (1987), for the thin plate, the elastic modulus of the piezoelectric layer are expressed as

$$\overline{c}_{11}^{E} = \frac{s_{11}^{E}}{(s_{11}^{E})^2 - (s_{12}^{E})^2} \tag{4.8}$$

$$\overline{c}_{12}^{E} = -\frac{s_{12}^{E}}{(s_{11}^{E})^2 - (s_{12}^{E})^2} \tag{4.9}$$

The piezoelectric constant and the relative permittivity at constant strain are respectively as

$$\overline{e}_{31} = \overline{e}_{32} = \frac{d_{31}}{s_{11}^{E} + s_{12}^{E}} \tag{4.10}$$

$$\overline{\varepsilon}_{33}^{S} = \overline{\varepsilon}_{33}^{T} - \frac{2d_{31}^{2}}{s_{11}^{E} + s_{12}^{E}} \tag{4.11}$$

4.2 Governing Equation in a Mechanical Domain

4.2.1 Equivalent Single-Layer Assumption

Because the two layers of the EH skin are assumed to be perfectly bonded to each other by strong conductive adhesives, it can be considered as an equivalent single layer. In this case, the equivalent flexural rigidity of the EH skin which consists of two-layer can be expressed as [63]

$$\mathrm{D}=\frac{1}{3}\left[c_{11}^{E}h_p^3+\frac{Y_s h_s^3}{1-\nu_s^2}\right]-\frac{\left[c_{11}^{E}h_p^2-\frac{Y_s h_s^2}{1-\nu_s^2}\right]^2}{4\left(c_{11}^{E}h_p+\frac{Y_s h_s}{1-\nu_s^2}\right)} \tag{4.12}$$

The equivalent density is calculated as

$$\rho=\rho_s h_s+\rho_p h_p \tag{4.13}$$

4.2.2 Base Excitation Assumption

The absolute displacement of the EH skin can be assumed to be the superposition of the base displacement and the relative displacement under the assumption of the base excitation [62].

$$w(x,y,t)=w_b(x,y,t)+w_{rel}(x,y,t) \tag{4.14}$$

4.2.3 Mechanical Equation of Motion

In the mechanical domain, the generalized Hamilton's principle was used to derive the mechanical equation of motion for forced damped vibration as

$$\begin{aligned}&\rho\ddot{w}_{rel}+\alpha\rho\dot{w}_{rel}+\beta\mathrm{D}\left(\frac{\partial^4\dot{w}_{rel}}{\partial x^4}+2\frac{\partial^4\dot{w}_{rel}}{\partial x^2\partial y^2}+\frac{\partial^4\dot{w}_{rel}}{\partial y^4}\right)\\&+\mathrm{D}\left(\frac{\partial^4 w_{rel}}{\partial x^4}+2\frac{\partial^4 w_{rel}}{\partial x^2\partial y^2}+\frac{\partial^4 w_{rel}}{\partial y^4}\right)\\&-\vartheta_s\upsilon(t)\left\{\frac{\partial^2 H(x,y)}{\partial x^2}-\frac{\partial^2 H(x-a,y)}{\partial x^2}\right\}\left\{\frac{\partial^2 H(x,y)}{\partial y^2}-\frac{\partial^2 H(x,y-b)}{\partial y^2}\right\}\\&=-\rho\ddot{w}_b\end{aligned} \tag{4.15}$$

where ϑ_s is the electromechanical coupling, α and β are proportional

damping constants, $H(x,y)$ is the Heaviside function, and $\upsilon(t)$ is the output voltage response under the given vibration condition. In this case, the inertia force $\rho\ddot{w}_b$ of the EH skin is considered as an external force.

4.3 Levy Solution for Relative Displacement of the EH Skin

4.3.1 Levy's Method

In this study, the levy's method was used to solve the relative displacement of the EH skin in Eq. (4.15). The Levy solution is a series solution involving the Fourier trigonometric functions as [46].

$$W_{rn}(x,y) = \sum_{n=1}^{k} Y_n(y)\sin\left(\frac{r\pi x}{a}\right) \tag{4.16}$$

It can be applied only to the rectangular plate where at least two opposite edges are simply supported.

4.3.2 Natural Frequencies and Model Shapes

In this study, for the free vibration analysis, the boundary condition of the EH skin is divided into two categories: 1) fully simply supported case and 2) fully clamped case.

Fully Simply Supported Case

In order to accomplish the Levy solution, a trigonometric series which satisfies the given boundary conditions should be founded. For a fully simply supported plate, the natural frequencies and mode shapes, obtained by the Levy's method, are

given as [59]

$$\omega_{rn} = \lambda^2 \sqrt{\frac{\mathrm{D}}{\rho}}, \qquad \left(\lambda^2 = \pi^2 \left\{ \left(\frac{r}{a} \right)^2 + \left(\frac{n}{b} \right)^2 \right\} \right) \tag{4.17}$$

$$W_{rn}(x, y) = A_{rn} \sin\left(\frac{r\pi x}{a} \right) \sin\left(\frac{n\pi y}{b} \right) \tag{4.18}$$

where λ is the eigenvalue which comes from the characteristic equation. A_{rn} is the mass normalized amplitude which is obtained by the orthogonality condition in Section 4.5.

Figure 4-2 shows the (1,1) mode of the EH skin which is the 1st symmetric mode under the fully simply supported boundary condition. The fundamental natural frequency was calculated to be 115.82 Hz.

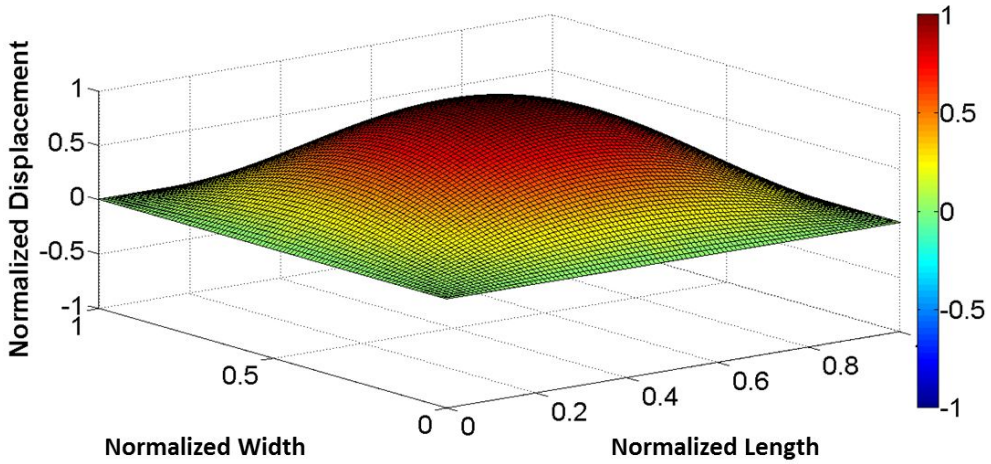

Figure 4-2 The 1st Symmetric Mode Shape of the EH Skin under the Fully Simply Supported Boundary Condition

Fully Clamped Case

In this section, the superposition method, developed by D. J. Gorman, was employed to calculate the natural frequencies and mode shapes of the fully clamped EH skin which do not have at least one pair of opposite edges simply supported, since the Levy solution cannot directly handle it.

Figure 4-3 shows two building blocks for analyzing the doubly symmetric modes of the fully clamped EH skin. Only a quarter segment of the fully clamped EH skin is analyzed.

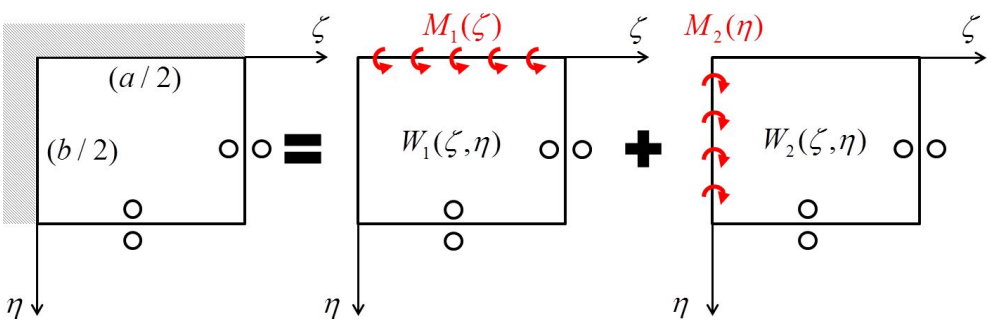

Figure 4-3 Superposition Method for the Fully Clamped Conditions

The circles, attached to the non-clamped edges of the quarter plate, indicate that there is no vertical edge reaction and the slope normal to these edges ($\zeta = 1$, $\eta = 1$) is zero. Furthermore, there is no displacement and the bending moment $M_1(\zeta)$ should be equal to the local bending moment along the edge $\eta = 0$ [65]. Therefore, the boundary conditions at one pair of opposite edges ($\eta = 0$, $\eta = 1$) are identified and the Levy's method can be applied to obtain the solution of the 1st building block. The Levy solution for the 1st building block $W_1(\zeta,\eta)$ is expressed as [65]

$$W_1(\zeta,\eta)$$
$$= \sum_{m=1,3,5}^{k^*} \frac{E_m}{\cos\gamma_m(\gamma_m^2+\beta_m^2)}\left\{\cos\gamma_m(1-\eta)-\frac{\cos\gamma_m}{\cosh\beta_m}\cosh\beta_m(1-\eta)\right\}\sin\frac{m\pi\zeta}{2} \quad (4.19)$$
$$-\sum_{m=k^*+2}^{2k-1} \frac{E_m}{\cosh\gamma_m(\gamma_m^2-\beta_m^2)}\left\{\cosh\gamma_m(1-\eta)-\frac{\cosh\gamma_m}{\cosh\beta_m}\cosh\beta_m(1-\eta)\right\}\sin\frac{m\pi\zeta}{2}$$

where

$$\beta_m = \phi\sqrt{\lambda^2+(m\pi/2)^2} \quad (4.20)$$

$$\gamma_m = \begin{cases} \phi\sqrt{\lambda^2-(m\pi/2)^2} & \left(\lambda^2 \geq (m\pi/2)^2\right) \\ \phi\sqrt{(m\pi/2)^2-\lambda^2} & \left(\lambda^2 \leq (m\pi/2)^2\right) \end{cases} \quad (4.21)$$

By following the similar procedures, the Levy solution for 2nd building block $W_2(\xi,\eta)$ is expressed as [65]

$$W_2(\xi,\eta)$$
$$= \sum_{n=1,3,5}^{k^*} \frac{E_n}{\cos\gamma_n(\gamma_n^2+\beta_n^2)}\left\{\cos\gamma_n(1-\zeta)-\frac{\cos\gamma_n}{\cosh\beta_n}\cosh\beta_n(1-\zeta)\right\}\sin\frac{n\pi\eta}{2} \quad (4.22)$$
$$-\sum_{n=k^*+2}^{2k-1} \frac{E_n}{\cosh\gamma_n(\gamma_n^2-\beta_n^2)}\left\{\cosh\gamma_n(1-\zeta)-\frac{\cosh\gamma_n}{\cosh\beta_n}\cosh\beta_n(1-\zeta)\right\}\sin\frac{n\pi\eta}{2}$$

where

$$\beta_n = (1/\phi)\sqrt{\lambda^2\phi^2+(n\pi/2)^2} \quad (4.23)$$

$$\gamma_n = \begin{cases} (1/\phi)\sqrt{\lambda^2\phi^2-(n\pi/2)^2} & \left(\lambda^2\phi^2 \geq (n\pi/2)^2\right) \\ (1/\phi)\sqrt{(n\pi/2)^2-\lambda^2\phi^2} & \left(\lambda^2\phi^2 \leq (n\pi/2)^2\right) \end{cases} \quad (4.24)$$

Finally, the solutions for each building block are superimposed on the original plate in dimensionless coordinates as

$$W_{rn}(\xi,\eta) = W_1(\xi,\eta) + W_2(\xi,\eta) \tag{4.25}$$

where $W_{rn}(\xi,\eta)$ is the mode shape of relative displacement of the EH skin for the fully clamped case.

Because there are k unknowns in each building block, $2k$ homogeneous algebraic equations for coefficients E_m and E_n should be solved. As a result, these algebraic equations are formulated by a matrix for an eigenvalue problem. In this study, λ^2 of 8.996 is the eigenvalue for the 1st doubly symmetric mode of the fully clamped EH skin when aspect ratio is one. Finally, the fundamental natural frequency was calculated to be 211.14 Hz.

4.4 Electrical Circuit Equation

According to Eq. (2.2), the electric displacement component can be expressed in terms of piezoelectric constant and permittivity at constant strain.

$$D_3 = \overline{e}_{31} S_1 + \overline{e}_{31} S_2 + \varepsilon_{33}^S E_3 \tag{4.26}$$

where S_1 and S_2 are strain components. Then, electric current can be obtained by substituting Eq. (4.7) and Eq. (4.26) into the Gauss's law in Eq. (2.3) as

$$
\begin{aligned}
&\frac{d}{dt}\left(\int_A \boldsymbol{D}\cdot\boldsymbol{n}dA\right)\\
&=\frac{d}{dt}\left(\int_A D_3 dA\right)\\
&=\frac{d}{dt}\left\{\int_A (\overline{e}_{31}S_1+\overline{e}_{31}S_2+\varepsilon_{33}^S E_3)dA\right\}\\
&=-\overline{e}_{31}h_{pc}\int_A\left\{\frac{\partial^3 w_{rel}(x,y,t)}{\partial x^2\partial t}+\frac{\partial^3 w_{rel}(x,y,t)}{\partial y^2\partial t}\right\}dA-\frac{\varepsilon_{33}^S ab}{h_p}\left(\frac{d\upsilon(t)}{dt}\right)\\
&=\frac{\upsilon(t)}{R_{load}}
\end{aligned}
\tag{4.27}
$$

where h_{pc} is the distance from the center of the piezoelectric layer to the neutral axis z_o which can be expressed as [66]

$$
z_o=\frac{c_{11}^E h_p^2-\left(\frac{Y_s h_s^2}{1-\nu_s^2}\right)}{2\left(c_{11}^E h_p-\left(\frac{Y_s h_s}{1-\nu_s^2}\right)\right)} \tag{4.28}
$$

Finally, the electrical circuit equation can be derived by integrating the Gauss's law and electric displacement component [62].

$$
C_p\frac{d\upsilon(t)}{dt}+\frac{\upsilon(t)}{R_l}=\vartheta_s\int_A\left\{\frac{\partial^3 w_{rel}(x,y,t)}{\partial x^2\partial t}+\frac{\partial^3 w_{rel}(x,y,t)}{\partial y^2\partial t}\right\}dA \tag{4.29}
$$

where C_p is a capacitance and expressed as

$$
C_p=\frac{\varepsilon_{33}^S ab}{h_p} \tag{4.30}
$$

4.5 Analytical Model of the EH Skin

4.5.1 Mechanical equation of Motion in Modal Coordinates

Orthogonality conditions can be applied to solve the forced vibration in modal coordinates.

$$\int_0^b \int_0^a W_{rn}(x,y)\left(\rho_s h_s + \rho_p h_p\right) W_{rn}(x,y)dxdy = 1 \tag{4.31}$$

$$\int_0^b \int_0^a W_{rn}(x,y)\mathrm{D}\left(\frac{\partial^4 \dot{w}_{rel}}{\partial x^4} + 2\frac{\partial^4 \dot{w}_{rel}}{\partial x^2 \partial y^2} + \frac{\partial^4 \dot{w}_{rel}}{\partial y^4}\right) W_{rn}(x,y)dxdy = \omega_{rn}^2 \tag{4.32}$$

$$Q(t) = -\rho A(t)\int_0^b \int_0^a W_{rn}(x,y)dxdy \tag{4.33}$$

where $A(t)$ is the input acceleration.

According to the orthogonal conditions, damping coefficient can be represented as a linear combination in terms of the mass and the stiffness under the assumption of the proportional damping as [59]

$$c = \alpha(\rho_s h_s + \rho_p h_p) + \beta\mathrm{D}\left(\frac{\partial^4 \dot{w}_{rel}}{\partial x^4} + 2\frac{\partial^4 \dot{w}_{rel}}{\partial x^2 \partial y^2} + \frac{\partial^4 \dot{w}_{rel}}{\partial y^4}\right) \tag{4.34}$$

$$\alpha + \beta\omega_{rn}^2 = 2\zeta_{rn}\omega_{rn} \tag{4.35}$$

The relative displacement can be represented by the mode shape of the EH skin using the modal expansion.

$$w_{rel}(x,y,t) = \sum_{r=1}^{\infty}\sum_{n=1}^{\infty} W_{rn}(x,y)\mu_{rn}(t) \tag{4.36}$$

where $W_{rn}(x,y)$ is normal modes which is obtained in Section 4.3.2 and $\mu_{rn}(t)$ is the

modal mechanical response function . Therefore, the mechanical equation of motion in modal coordinates can be obtained as

$$\frac{\partial^2 \mu_{rn}(t)}{\partial t^2} + 2\zeta_{rn}\omega_{rn}\frac{\partial \mu_{rn}(t)}{\partial t} + \omega_{rn}^2 \mu_{rn}(t) - \theta \vartheta_s = Q(t) \tag{4.37}$$

4.5.2 Electrical Circuit Equation in Modal Coordinates

In modal coordinates, the modal electromechanical coupling, denoted by θ, related to energy conversion efficiency from vibration energy to electrical energy is defined as [34]

$$\theta = -\bar{e}_{31} h_{pc} \int_0^b \int_0^a \left\{ \frac{\partial^2 W_{rn}(x,y)}{\partial x^2} + \frac{\partial^2 W_{rn}(x,y)}{\partial y^2} \right\} dxdy \tag{4.38}$$

By substituting Eq. (4.36) and Eq. (4.38) into Eq. (4.29), therefore, the electrical circuit equation can be obtained in modal coordinates as [34].

$$C_p \frac{d\upsilon(t)}{dt} + \frac{\upsilon(t)}{R_{load}} - \sum_{r=1}^{\infty}\sum_{n=1}^{\infty} \theta \frac{d\mu_{rn}(t)}{dt} = 0 \tag{4.39}$$

4.5.3 Steady-State Voltage Response

The output voltage response of the EH skin was obtained by solving the mechanical equation of motion and the electrical circuit equations simultaneously as [34]

$$\upsilon(\omega) = \frac{\left(j\omega R_{load}\theta\right) A}{\left(1 + j\omega R_{load}\frac{C_p}{2}\right)\left(\omega_{rn}^2 - \omega^2 + j2\zeta_{rn}\omega_{rn}\omega\right) + j\omega R_{load}\theta^2} \tag{4.40}$$

4.6 Electric Power Prediction

In this analytical study, the size of the EH skin was 10 cm^2 and acceleration amplitude was 0.5 g level. Table 2 shows the mechanical and electrical parameters of the EH skin.

Table 2 Mechanical and Electrical Parameters of the EH Skin

Mechanical Parameters		**Electrical Parameters**	
c_{11}^E	66.16 GPa	d_{31}	-2.74×10^{-10} m/V
c_{12}^E	19.17 GPa	e_{31}	-23.38 C/m^2
c_{66}^E	23.47 GPa	ε_0	8.854 pF/m
Y_s	124 GPa	ε_{33}^T	30.10 nF/m
h_p	0.2667 mm	ε_{33}^S	17.29 nF/m
h_s	0.1016 mm	C_p	648.18 nF
ρ_p	7500 kg/m^3	$R_{load}^{short,FSS}$	677.90 Ω
ρ_s	7800 kg/m^3	$R_{load}^{open,FSS}$	6033.09 Ω
$1/(2\zeta)$	30	$R_{load}^{short,FC}$	464.20 Ω
a	100 mm	$R_{load}^{open,FC}$	2705.70 Ω
b	100 mm		

4.6.1 Fully Simply Supported Case

Short-Circuit Resonance

Figure 4-4 shows a frequency sweep for the electric power response in the resonance case. The peak appears at short-circuit resonance frequency of 116.3 Hz. The optimal resistance was found by external loading variation. With 677.90 Ω, the peak electric power was 4.5 mW.

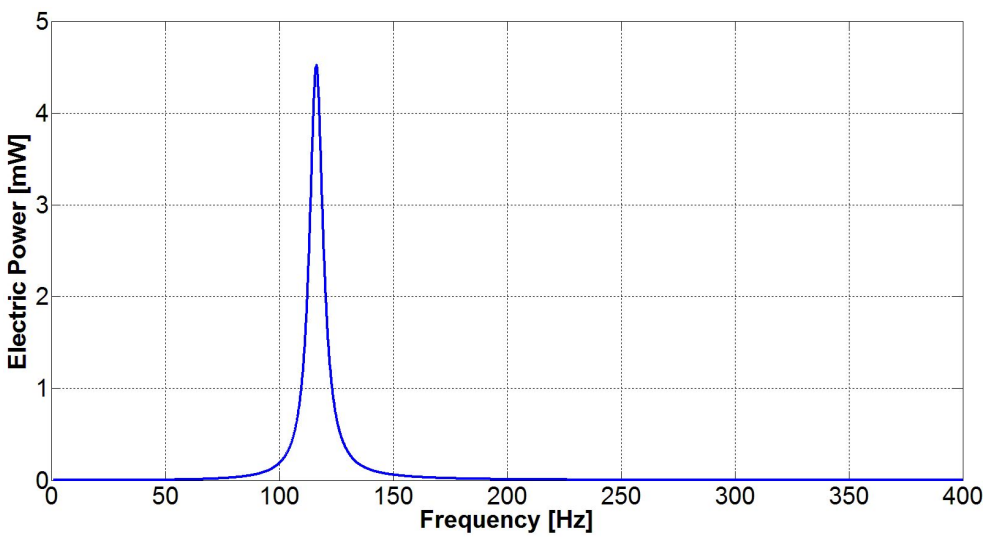

Figure 4-4 Electric Power Prediction for Short-Circuit Resonance Frequency of Fully Simply Supported Case

Open-Circuit Resonance

The open-circuit resonance frequency was calculated to be 120.9 Hz. With the impedance matching of 6033.09 Ω, the peak electric power of each case is same, as shown in Figure 4-5. According to the relationship between frequency and impedance of piezoelectric materials, the current of the short-circuit resonance frequency is larger than that of the open-circuit resonance frequency. But the

voltage behaves inversely. That is why electric power in both cases is same.

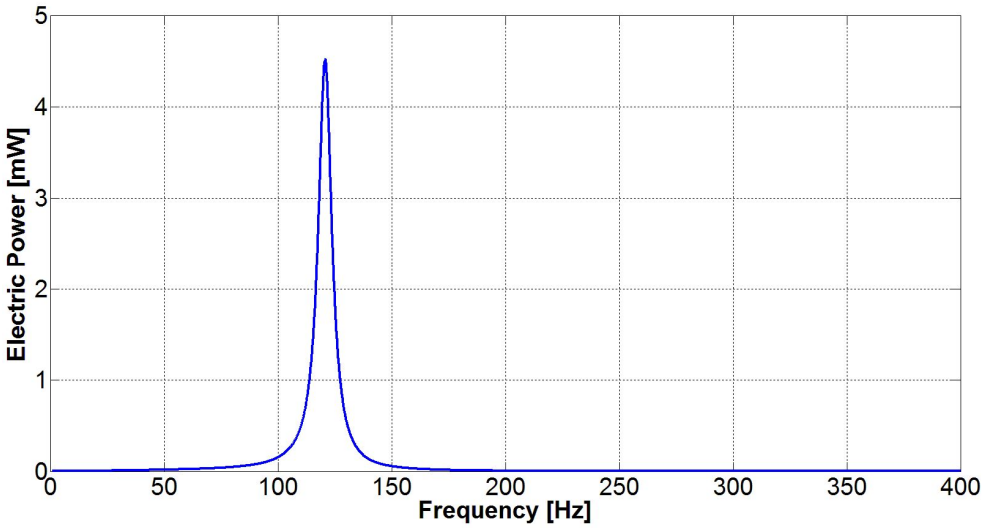

Figure 4-5 Electric Power Prediction for Open-Circuit Resonance Frequency of Fully Simply Supported Case

4.6.2 Fully Clamped Case

Short-Circuit Resonance

As shown in Figure 4-6, the maximum electric power of 1.83 mW was predicted at the short-circuit resonance frequency of 211.8 Hz. Because the fundamental natural frequency of the fully clamped is higher than that of the fully simply supported EH skin, electric power of the fully clamped is lower than that of fully simply supported EH skin. In addition, net electric power is reduced due to inflection lines along the edges in the fully clamped EH skin. This phenomenon will be explained in Section 4.7.

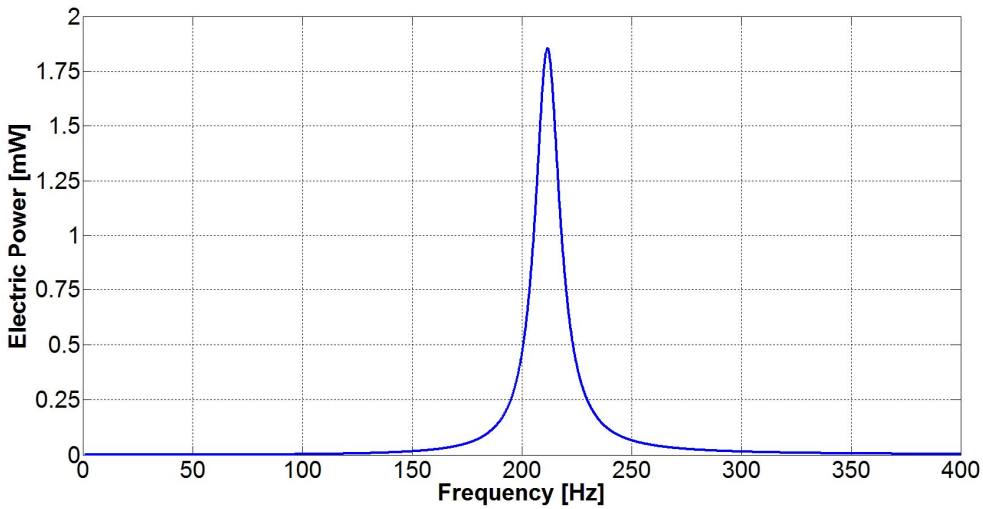

Figure 4-6 Electric Power Prediction for Short-Circuit Resonance Frequency of Fully Clamped Case

Open-Circuit Resonance

As shown in Figure 4-7, the maximum electric power of 1.83 mW was predicted at the short-circuit resonance frequency of 226.4 Hz. Like the fully simply supported case, electric power at the short-circuit and the open-circuit resonance frequency is same. Because the ratio of the short-circuit to the open-circuit resonance frequency depends on the modal electromechanical coupling, the capacitance, natural frequency, and modal damping ration [62], the amount of the resonance frequency shift is different from each other.

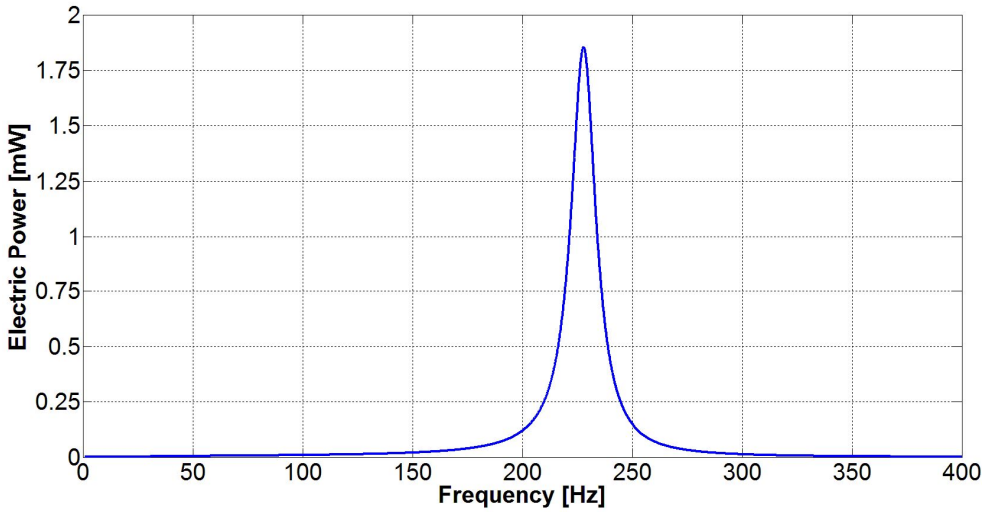

Figure 4-7 Electric Power Prediction for Open-Circuit Resonance Frequency of Fully Clamped Case

4.7 Inflection Line Extraction

4.7.1 Voltage Cancellation

According to Eq. (4.40) and Eq. (4.38), the output voltage response is proportional to the sum of the normal strain components S_1 and S_2. In other words, when the sum of the normal strain components is zero at an inflection line, there is no voltage generation. As the order of the vibration mode is gets higher, the curvature sign of the deflection changes along the inflection line and it reduces electric power generation. This phenomenon is called the voltage cancellation [1]. Fortunately, these inflection lines can be removed by piezoelectric material segmentation, proposed by S. Lee et al., as shown in Figure 4-8 [1] .

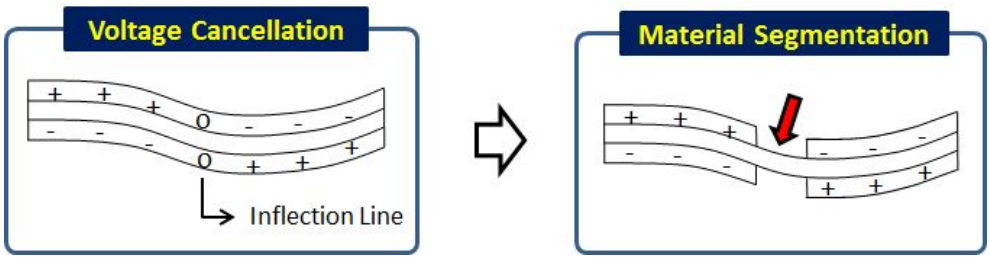

Figure 4-8 Piezoelectric Material Segmentation using the Inflection Line Extraction

The inflection lines can be extracted from the mode shape which is analyzed by the analytical model of the EH skin. Therefore, the developed analytical model of the EH skin can be used to inform the inflection lines for conceptual design for piezoelectric material segmentation. The following two subsections explain the guidelines of the inflection line extraction in the fully simply supported and fully clamped case respectively.

4.7.2 Inflection Lines in the Fully Simply Supported Case

In the 1st mode, the top and the bottom of the EH skin experience tension and compression respectively, as shown in Figure 4-9. Because there is no sign change of curvature in the 1st mode of the fully simply supported case, the inflection lines do not exist. As a result, the voltage cancellation does not occur in the 1st mode of the fully simply supported case.

However, the 2nd mode of the fully simply supported case is skew-symmetric about the inflection line (center line), as shown in Figure 4-10. It causes that electric power is totally eliminated.

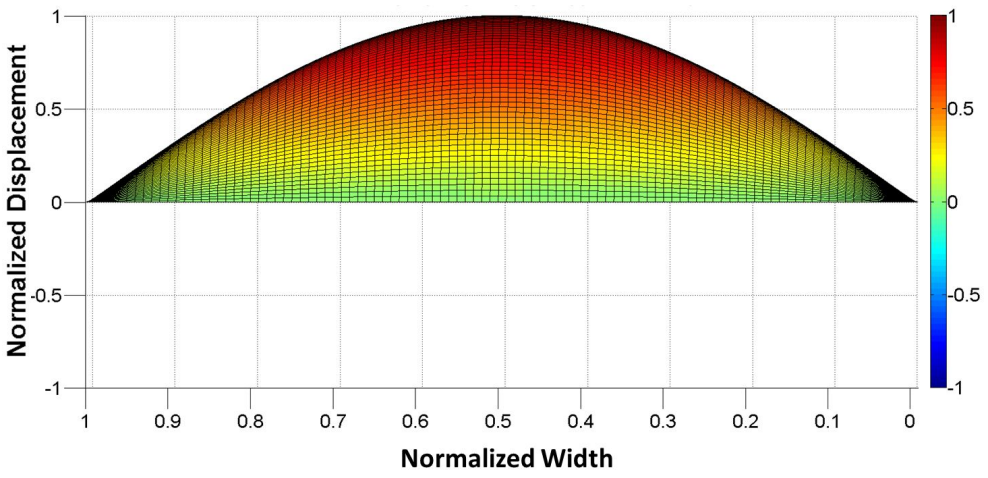

Figure 4-9 Curvature of the 1st Mode Shape of the Fully Simply Supported EH Skin

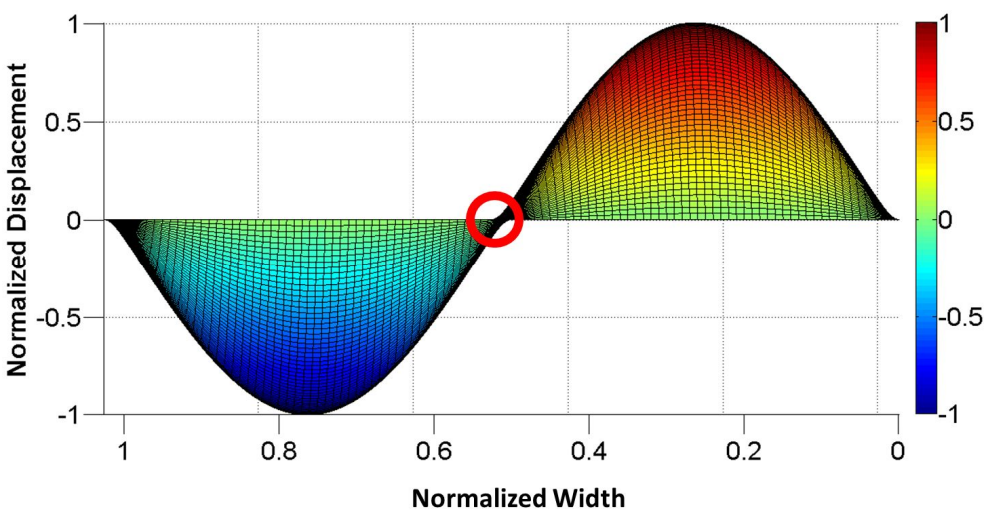

Figure 4-10 The Sign Change of the Curvature in the 2nd mode of the fully simply supported EH Skin

4.7.3 Inflection Lines in the Fully Clamped Case

The extraction of the inflection lines for the material segmentation design is more important in the fully clamped case. Figure 4-11 shows the 1st mode shape of the fully clamped EH skin.

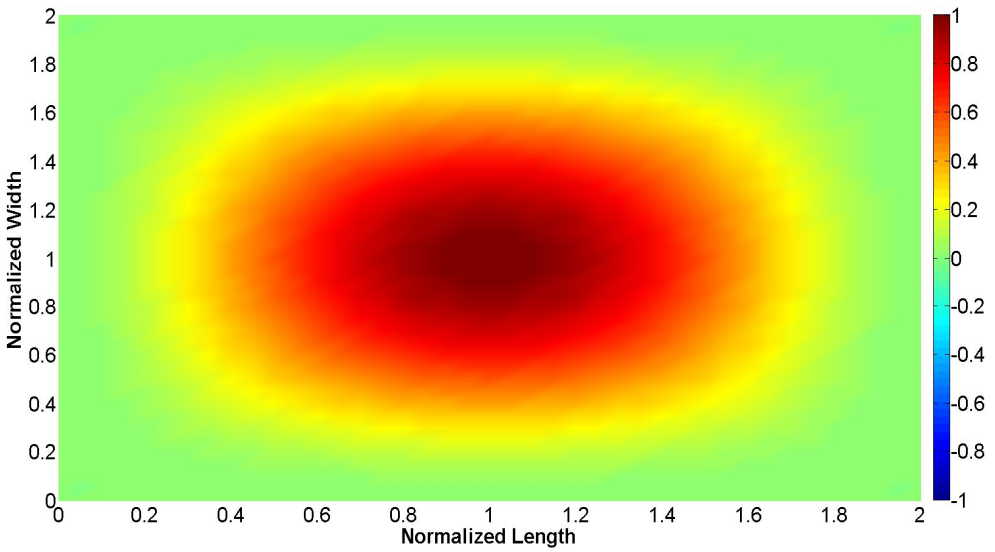

Figure 4-11 The 1st Mode Shape of the Fully Clamped EH Skin

Unlike the fully simply supported case, the 1st mode of the fully clamped has the curved inflection lines along the edges, as shown in Figure 4-12. Because the 1st mode has the majority of vibration energy, these inflection lines must be removed to improve the energy conversion efficiency.

Figure 4-13 shows the sum of the normal strain distribution in 3- dimensions. As mentioned in Section 4.7.1, because the voltage response is proportional to the sum of the normal strain distribution in the x-direction (Figure 4-12 (a)) and the y-direction (Figure 4-12 (b)), the inflection lines should be extracted from the sum of the normal strain distribution (Figure 4-14 (b)).

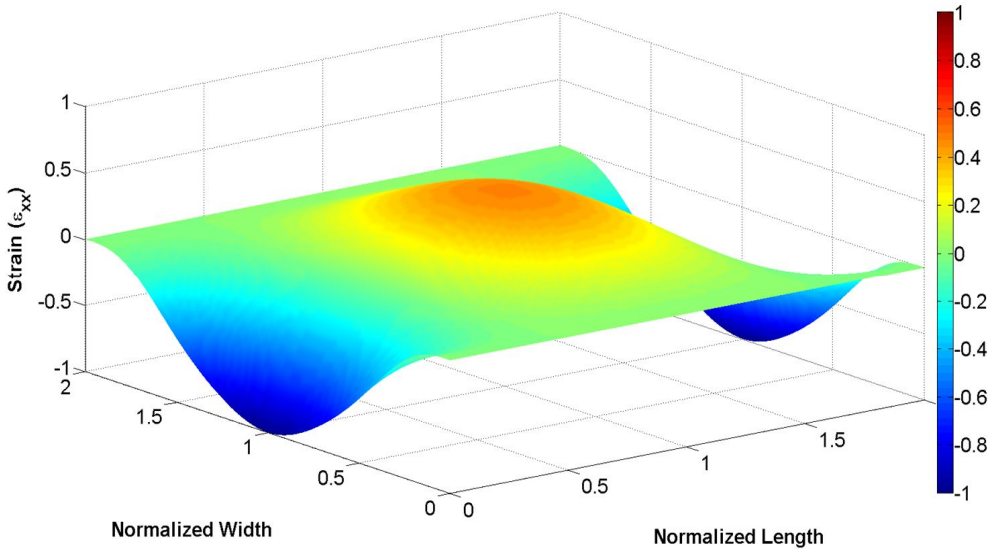

(a)Normal Strain Distribution in the x-direction

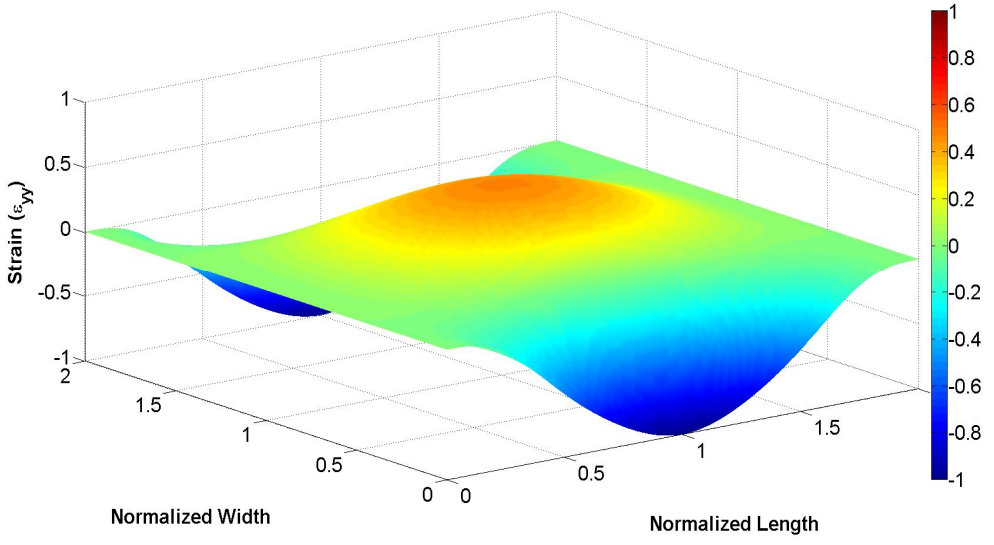

(b) Normal Strain Distribution in the y-direction

Figure 4-12 Normal Strain Distribution of the Fully Clamped EH Skin

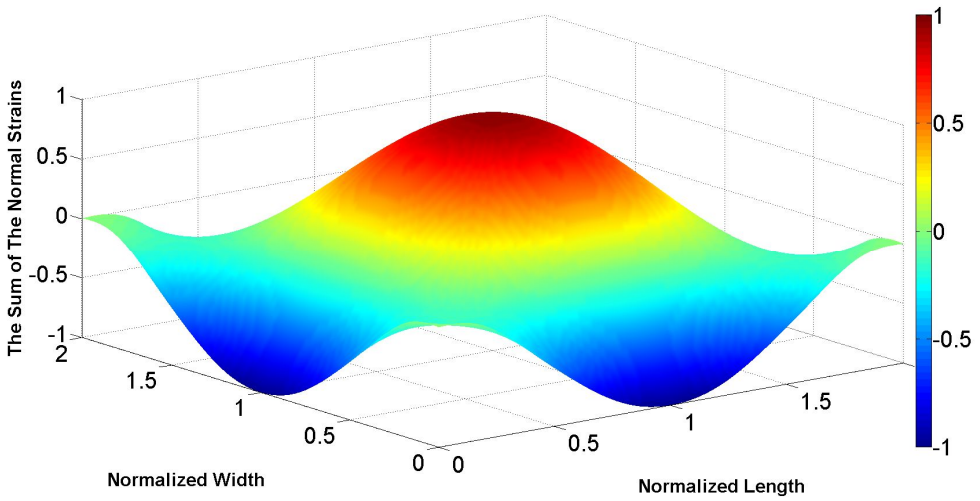

Figure 4-13 The Sum of the Normalized Normal Strains (3D)

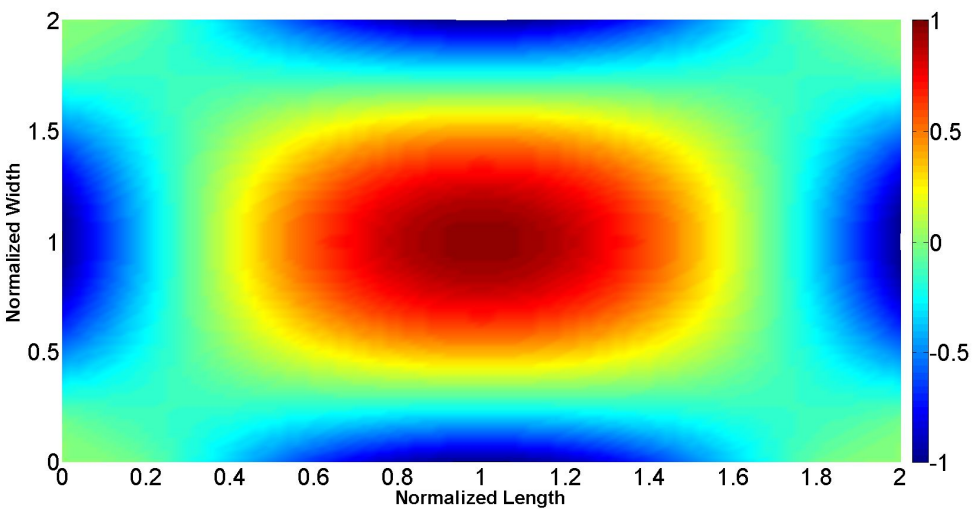

Figure 4-14 The Sum of the Normalized Normal Strains (2D)

Chapter 5. Conclusions and Discussions

5.1 Contributions

This study aims at developing the analytical model of the piezoelectric energy harvester for electric power prediction and conceptual design. This study is composed of two research thrusts: (1) stochastic analysis of harvestable expected electric power and (2) electromechanically coupled analytical model of the EH skin. It is expected that this research offers the following potential contributions in the piezoelectric energy harvesting field:

- **Contribution 1: Stochastic analysis of harvestable electric power under non-stationary random vibrations**

By applying statistical time-frequency analysis to extract stochastic information of non-stationary random vibrations, the expected electric power can be predicted when statistical moments randomly change with time. As long as the time-frequency representation is an unbiased estimator under the given vibration condition, the variation of harvestable electric power can be accurately visualized for any kinds of non-stationary random vibration in a stochastic manner. To the best of the author's knowledge, this is the first study of piezoelectric energy harvesting analysis with the time-frequency representation to estimate the time-varying PSD. In addition, expected electric power prediction from realistic random vibration signals of mechanical equipment can confirm whether it is feasible or not to operate target applications such as wireless sensors for structural health monitoring and building automation in real world. Furthermore, the proposed

framework can lead to a robust design of piezoelectric energy harvester for reliably scavenging high electric power considering random nature.

- **Contribution 2: Electromechanically coupled analytical model of the EH skin**

The electromechanically coupled analytical model of the EH skin using the Kirchhoff plate theory was developed. Electric power at the short-circuit resonance and open-circuit resonance frequency was predicted for the fully simply supported and fully clamped cases. Besides, the electromechanical behavior of the EH skin is theoretically investigated. Furthermore, the developed analytical model can be used to extract the inflection lines for material segmentation to avoid the voltage cancellation and gives the guideline for conceptual design of the EH skin.

5.2 Future Works

Although the analytical models developed in this thesis successfully address some challenges in piezoelectric energy harvesting, there are still several research topics that further investigations and advances are required to bring it into an alternative solution for powering wireless sensor networks or low-power electronics.

- **Suggestion 1: Verification and validation of the analytical model**

The uncertainty always exists in physical properties, such as the manufacturing tolerance, the thickness, the piezoelectric strain coefficient, the relative permittivity, and the elastic modulus of piezoelectric layer and substrate layer. To enhance the

predictive capability of the analytical model, therefore, a statistical calibration is needed to determine valid mechanical and piezoelectric properties through a comparison of the predicted and observed responses.

- **Suggestion 2: Inflection lines extraction considering an electrical load**

There is the backward electromechanical coupling induced in the piezoelectric energy harvester by the inverse piezoelectric effect. Therefore, the resonance frequency shift as well as dynamic strain distributions from the mode shape should be considered to extract the inflection lines.

- **Suggestion 3: Reliability-based optimal number and locations of piezoelectric materials**

The optimal number and locations of the EH materials are required to reliably scavenge high electric power output for least cost. In this study, the piezoelectric layer was assumed to be fully covered on the surface of the vibrating structure. However, if piezoelectric patches are selectively attached on the local regions which experience high dynamic strain, the EH skin can be efficiently utilized.

Bibliography

1. S. Lee, B. D. Youn, and B. C. Jung, 2009, "Robust segment-type energy harvester and its application to a wireless sensor," *Smart Materials and Structures*, Vol. 18, No. 9

2. T. Ikeda, 1990, "Fundamentals of Piezoelectricity," Oxford University Press Inc

3. 1987, *IEEE Standard on Piezoelectricity*, IEEE, New York

4. R. Holland and E. P. EerNisse, 1969, "Design of Resonant Piezoelectric Devices," The Massachusetts Institute of Technology

5. R. G. Ballas, 2007, "Piezoelectric Multilayer Beam Bending Actuators," Springer

6. H. A. Sodano, D. J. Inman, and G. Park, 2004, "A Review of Power Harvesting form Vibration Using Piezoelectric Materials," *The Shock and Vibration Digest*, Vol. 36, No. 3, pp. 197, 205.

7. S. R. Anton and H. A. Sodano, 2007, "A review of power harvesting using piezoelectric materials," *Smart Materials and Structures*, Vol. 16, No. 3

8. S. P. Beeby, R. N. Torah, M. J. Tudor, P. Glynne-Jones, T. O'Donnell, and S. Roy, 2007, "A micro electromagnetic generator for vibration energy harvesting," *Journal of Micromechanics and Microengineering,* Vol. 17, pp. 1257-1265

9. S. P. Beeby, M. J. Tudor, R. N. Torah, S. Roberts, T. O'Donnell, and S. Roy, 2007, "Experimental comparison of macro and micro scale electromagnetic vibration powered generators," *Microsystem Technologies,* Vol. 13, pp. 1647-1653

10. E. O. Torres, and G. A. Rincón-Mora, 2009 "Electrostatic energy-harvesting and battery-charging CMOS system prototype," *IEEE Transactions on Circuits and Systems I: Regular Papers,* Vol. 56, No. 9, pp. 1938-1948

11. M. Lallart, S. Pruvost, and D. Guyomar, 2011, "Electrostatic energy harvesting enhancement using variable equivalent permittivity," *Physics Letters A*.

12. L. Wang and F. G. Yuan, 2008, "Vibration energy harvesting by magntostrictive material," *Smart Materials and Structures*, Vol. 17, No. 4

13. A. Adly, D. Davino, A. Giustiniani, and C. Visone, 2010 "Experimental tests of a magnetostrictive energy harvesting device toward its modeling," *Journal of Applied Physics*, Vol. 107, No. 9

14. L. Wang and F. G. Yuan, 2007, "Energy harvesting by magnetostrictive material (MsM) for powering wireless sensors in SHM," *SPIE Smart Structures and Materials & NDE and Health Monitoring*, 14th International Symposium, pp.18-22

15. S. Roundy, E. S. Leland, J. Baker, E. Carleton, E. Reilly, E. Lai, B. Otis, J. M. Rabaey, P. K. Wright, and V. Sundararajan, 2005, "Improving power output for vibration-based energy scavengers," *Pervasive Computing*, Vol. 4, No. 1.

pp. 28-36

16. M. Kim, S. Hong, D. J. Miller, J. Dugundji, and B. L. Wardle, 2011, "Size effect of flexible proof mass on the mechanical behavior of micron-scale cantilevers for energy harvesting applications," *Applied Physics Letters*, Vol. 99, No. 24

17. F. Goldschmidtboeing and P. Woias, 2008, "Characterization of different beam shapes for piezoelectric energy harvesting," *Journal of Micromechanics and Microengineering*, Vol. 18, No. 10

18. S. Lee and B. D. Youn, 2011, "A New Piezoelectric Energy Harvesting Design Concept; Multimodal Energy Harvesting Skin," *IEEE Transactions on Ultrasonics, Ferroelectrics, and Frequency Control*, Vol.58, No.3, pp.629-645

19. M. Lallart, S. R. Anton, and D. J. Inman, 2010, "Frequency self-tuning scheme for broadband vibration energy harvesting," *Journal of Intelligent Material Systems and Structures*, Vol. 21, pp. 897-906

20. S. Qi, R. Shuttleworth, S. O. Oyadiji, and J. Wright, 2010, "Design of a multiresonant beam for broadband piezoelectric energy harvesting," *Smart Materials and Structures*, Vol. 19

21. W. Al-Ashtari, M. Hunstig, T. Hemsel, and W. Sextro, 2012, "Frequency tuning of piezoelectric energy harvesting by magnetic force," *Smart Materials and Structures*, Vol. 21

22. X. Chen, S. Xu, N. Yao, and Y. Shi, 2010, "1.6 V Nanogenerator for Mechanical Energy Harvesting Using PZT Nanofibers," *Nano Letters*, Vol. 10, No. 6, pp. 2133-2137

23. Y. Qi, N. T. Jafferis, K. Lyons, C. M. Lee, H. Ahmad, and M. C. McAlpine, 2010, "Piezoelectric Ribbons Printed onto Rubber for Flexible Energy Conversion," *Nano Letters*, Vol. 10, No. 2, pp. 524-528

24. Y. Qi, J. Kim, T. D. Nguyen, B. Lisko, P. K. Purohit, and M. C. McAlpine, 2011, "Enhanced piezoelectricity and stretchability in energy harvesting devices fabricated from buckled PZT ribbons," *Nano letters*, Vol. 11, No. 3, pp. 1331-1336.

25. G. Y. Yun, J. H. Kim, and J. Kim, 2009, "Dielectric and polarization behaviour of cellulose electro-active paper (EAPap)," *Journal of Physics D: Applied Physics*, Vol. 42 No. 8

26. G. K. Ottman, H. F. Hofmann, and G. A. Lesieutre, 2003, "Optimized piezoelectric energy harvesting circuit using step-down converter in discontinuous conduction mode," *IEEE Transactions on Power Electronics*, Vol. 18, No. 2, pp. 696-703

27. M. J. Guan and W. H. Liao, 2007 "On the efficiencies of piezoelectric energy harvesting circuits towards storage device voltages," *Smart Materials and Structures,* Vol. 16

28. S. Lee, B. D. Youn, and M. Giraud, "Designing energy harvesting skin

structure utilizing outdoor unit vibration," *ASME International Design Engineering Technical Conf. & Computers and Information in Engineering Conference*, Montreal, Canada, 2010, Art. No. DETC2010-29180.

29. S. W. Arms, C. P. Townsend, D. L. Churchill, J. H. Galbreath, and S. W. Mundell, 2005, "Power management for energy harvesting wireless sensors," *In Proceedings on SPIE*, Vol. 5763, pp. 267-275

30. S. Roundy and P. K. Wright, 2004, "A piezoelectric vibration based generator for wireless electronics," *Smart Materials and Structures*, Vol. 13, No. 5

31. H. A. Sodano, G. Park, and D. J. Inman, 2004, "Estimation of Electric Charge Output for Piezoelectric Energy Harvesting," *Journal of Strain*, Vol. 40 pp. 49-58

32. A. Erturk and D. J. Inman, 2008, "On mechanical modeling of cantilevered piezoelectric vibration energy harvesters," *Journal of Intelligent Material Systems and Structures*, Vol. 19, pp. 1311-1325

33. N. E. duToit and B. Wardle, 2007, "Experimental Verification of Models for Microfabricated Piezoelectric Vibration Energy Harvesters," *AIAA Journal*, Vol. 45, No. 5, pp. 1126-1137

34. A. Erturk and D. J. Inman, 2009, "An experimentally validated bimorph cantilever model for piezoelectric energy harvesting from base excitations," *Smart Materials and Structures*, Vol. 18, No. 2

35. N. E. DuToit, B. L Wardle, and S. Kim, 2005, "Design Considerations for

MEMS-Scale Piezoelectric Mechanical Vibration Energy Harvesters," *Integrated Ferroelectrics*, Vol. 71, pp. 121-160

36. E. Halvorsen, 2008, "Energy Harvesters driven by broadband random vibrations," *Journal of Microelectromechanical Systems*, Vol. 17, No. 5, pp. 1061-1071

37. S. Adhikari and D. J. Inman, 2009, "Piezoelectric energy harvesting from broadband random vibrations," *Smart Materials and Structures*, Vol. 18, No. 11

38. T. Seuaciuc-Osorio and M. F. Daqaq, 2010, "Energy harvesting under excitations of time-varying frequency," *Journal of Sound and Vibrations*, Vol. 329, pp. 2497-2515.

39. S. F. Ali, S. Adhikari, and M. I. Friswell, 2011, "Analysis of magnetopiezoelastic energy harvesters under random excitations: an equivalent linearization approach," *Proceedings of SPIE 7977, Active and Passive Smart Structures and Integrated Systems 2011,* Vol. 7977, 79770N

40. S. Zhao and A. Erturk, 2013, "Electroelastic modeling and experimental validations of piezoelectric energy harvesting from broadband random vibrations of cantilevered bimorphs," *Smart Materials and Structures*, Vol. 22

41. C. J. Rupp, A. Evgrafov, K. Maute, and M. L. Dunn, 2009, "Design of piezoelectric energy harvesting systems: A topology optimization approach based on multilayer plates and shells," *Journal of Intelligent Material Systems*

and Structures, Vol. 20, pp. 1923-1939

42. C. D. Marqui Junior, A. Erturk, and D. J. Inman, 2009, "An electromechanical finite element model for piezoelectric energy harvester plates," *Journal of Sound and Vibration*, Vol. 327, No. 1, pp. 9-25

43. S. Kim, W. W. Clark, and W. M. Wang, 2005, "Piezoelectric energy harvesting with a clamped circular plate: analysis," *Journal of Intelligent Material Systems and Structures*, Vol. 16, No. 10, pp. 847-854.

44. A. Erturk, 2011, "Piezoelectric energy harvesting for civil infrastructure system applications: Moving loads and surface strain fluctuations," *Journal of Intelligent Material Systems and Structures,* Vol. 22, No. 17, pp. 1959-1973

45. S. Yu and S. He, 2012, "Accurate free vibration analysis of cantilever piezoelectric panel carrying a rigid mass," *Journal of Vibration and Control*, DOI: 10.1177/1077546312444657

46. D. J. Gorman, 1976, "Free vibration analysis of cantilever plates by the method of superposition," *Journal of Sound and Vibration*, Vol. 49, pp. 453-467

47. J. A. Gubner, 2006, "Probability and Random Process for Electrical and Computer Engineers," Cambridge University Press

48. K. Shin and J. K. Hammond, 2008, "Fundamentals of Signal Processing for Sound and Vibration Engineers," John Wiley & Sons

49. L. Zhang, G. Xiong, H. Liu, H. Zou, and W. Guo, 2010, "Time-frequency representation based on time-averaging AR model with applications to non-stationary rotor vibration analysis," *Sadhana*, Vol. 35, Part 2, pp. 215-232.

50. A. G. Poulimenous and S. D. Fassois, 2006, "Parametric time-domain methods for non-stationary random vibration modeling and analysis," *Mechanical Systems and Signal Processing*, Vol. 20, No. 4, pp. 763-816

51. O. Bessen and F. Castanie, 1993, "On estimating the frequency of a sinusoid in autoregressive multiplicative noise," *Signal Processing*, Vol. 30, No. 1, pp. 65-83

52. MD. Khademul Islam Molla, and Keikichi Hirose, 2010, "Hilbert spectrum in Time-Frequency representation of audio signals considering disjoint orthogonality," *Advances in Adaptive Data Analysis*, Vol. 2, No. 3 pp. 313-336

53. P. Flandrin, 2003, "Time-Freuqnecy/Time-Scale Analysis," Academic Press

54. B. Boashash, 2003, "Time Frequency Signal Analysis and Processing," ElSEVIER

55. Tutorial, 2009, "The Fundamentals of FFT-Based Signal Analysis and Measurement in LabVIEW and LabWindows/CVI," NATIONAL INSTRUMENTS (NI)

56. P. Flandrin, F. Auger and E. Chassande-Mottin, 2003, "Time–frequency reassignment," CRC Press

57. J. Xiao et al., 2007, "Multitaper Time-Frequency reassignment for nonstationary spectrum estimation and chirp enhancement," *Signal Processing*, Vol. 55, No. 6, pp. 2851-2860

58. J. Li and J. Chen, 2009, "Stochastic Dynamics of Structures," John Wiley & Sons

59. S. S. Rao, 2007, "Vibration of Continuous System," John Wiley & Sons

60. L. Meirovitch, 2001, "Fundamentals of Vibrations," McGraw Hill

61. E. J. Haug and K. K. Choi, 1993, "Methods of Engineering Mathematics," Prentice Hall

62. A. Erturk and D. J. Inman, 2011, "Piezoelectric Energy Harvesting," John Wiley & Sons

63. R. Szilard, 2004, "Theories and Applications of Plate Analysis," John Wiley & Sons

64. A. Ugural, 2009, "Stresses in Beams, Plates, and Shells," CRC Press

65. D. J. Gorman. 1982, "The Free Vibration Analysis of Rectangular Plates," Elsevier

66. A. Y. Vyskrebentsev and A. I. Kholod, 1969, "Contribution to the bending theory of two layer plates," *Soviet Applied Mechanics,* Vol. 5, No. 2, pp. 392-397

국문 초록

최근 우리 주변에서 쉽게 버려지는 에너지를 수확해서 전력으로 재사용하는 에너지 하베스팅 기술이 많은 각광을 받고 있다. 이 중에서 진동을 이용하는 압전 에너지 하베스팅은 에너지 밀도가 높고 추가적인 보조 장치가 필요 없기 때문에, 기술적 실현 가능성이 높아 다양한 분야에서 연구들이 진행되고 있다. 기본적인 변환 원리는 응력에 의해 변형이 일어나면 전류가 발생하는 압전 효과를 이용한 것으로, 주어진 진동 조건에서 수확 가능한 전력을 극대화하는 최적 설계 및 전기-기계적 거동의 이해를 위해서는 압전 에너지 수확 장치의 해석적 수학 모델 개발이 필수적이다. 이에 본 논문에서는 1) 비정상 랜덤 진동에서 수확 가능한 전력의 통계적 예측, 2) 에너지 하베스팅 스킨의 이론 정립을 위한 해석적 수확 모델 개발을 목표로 하였다.

먼저 기존의 모델들은 일정한 주파수와 가속도를 갖는 조화함수로 가정된 결정론적 신호만을 다루기 때문에, 자연계에 존재하는 진동에 내포해 있는 불규칙성을 표현할 수 없다. 또한 랜덤 진동을 백색 Gaussian 잡음으로 가정하여 시불변 파워 스펙트럼 밀도를 계산하는 경우, 자기상관 함수와 같은 2차 모멘트가 시간에 따라 불규칙하게 변하는 비정상 랜덤 진동에는 적용할 수 없다. 따라서 상기된 문제점들을 해결하기 위해서, 본 논문의 첫 번째 연구에서는 통계적 시간-주파수 신호 처리 기법을 압전 에너지 하베스팅 해석에 최초로 적용하여, 비정상 랜덤 진동에 대한 수확 가능 전력의 통계적 해석 방법론을 총 3단계로 제안하였다. 1단계에서는 smoothed pseudo Wigner-Ville 분포를 이용하여 비정상 랜덤 진동의 시변 파워 스펙트럼 밀도를

추정한 후, 2단계에서 정의된 선형 전기-기계 시스템을 통해 3단계에서 전압 응답의 시편 파워 스펙트럼 밀도를 추정한다. 끝으로 전압 응답의 시변 파워 스펙트럼 밀도로부터 얻어진 전압 응답의 자기상관 함수를 통한 실시간 평균 전력 예측하였다.

두 번째 연구에서는, 기존의 외팔 보 형태의 압전 에너지 수확 장치의 한계를 극복하기 구조물에 압전 소재를 직접 부착하는 에너지 하베스팅 스킨의 해석적 수확 모델을 Kirchhoff 판 이론을 기반으로 유도하였다. 이를 위해, Erturk이 2009년에 개발한 1차원 외팔 보에 대한 전기-기계적 연성 모델을 2차원 판으로 확장하였다. Hamilton 원리를 통해 유도된 운동 방정식으로부터 기계적 변위와 모드 형상을 얻기 위해 Levy 해법을 사용하였으며, 모든 모서리가 클램핑된 판에 대해서는 중첩의 원리를 적용하였다. 또한 Gauss 법칙으로부터 얻어진 전기적 회로 방정식과 상기된 운동 방정식으로부터 최종적인 전압 예측 모델을 유도하였다. 끝으로 곡률의의 부호가 바뀌는 지점인 변곡선으로 인한 전압 상쇄 효과를 방지하기 위하여, 제시된 해석적 수확 모델을 통해 압전 재료의 분할 설계를 위한 가이드라인을 제시하였다.

주요어: 압전 에너지 하베스팅
비정상 랜덤 진동
통계적 시간-주파수 신호 처리
시변 파워 스펙트럼 밀도
Kirchhoff 판 이론
압전 소재 분할

학 번: 2011-20730

감사의 글

샬롬! 단기간에 최대의 이윤을 창출하는 것이 공학의 철학이지만, 제가 공부하는 이유는 오직 '이웃 사랑'을 실천하기 위해서입니다. 기계공학을 전공하면서 얻은 지식을 통하여 세상에 조금이나마 기쁨과 희망을 전해줄 수 있다면, 이것이야말로 저의 가장 큰 행복이고 소망입니다.

이러한 저의 비전을 이루기 위한 첫 걸음으로써, 2년의 석사과정 동안 연구한 내용들이 작은 결실을 맺어 한 편의 학위 논문으로 발표하게 되었습니다. 이를 위해 물심양면으로 지도해주시고 따뜻한 사랑으로 격려해 주신 윤병동 교수님께 진심으로 감사의 말씀을 전해 드립니다. 교수님의 가르침을 통해 냉철해진 두뇌와 연구를 향한 열정으로 뜨거워진 심장을 가지고 세상에 꼭 필요한 기술을 연구하는 참된 학자가 되겠습니다. 더불어 귀중한 시간에 심사를 맡아주신 신효철 교수님과 조맹효 교수님께도 깊은 감사를 드립니다.

한 사람이 꾼 꿈은 잠에서 깨어나면 기억에서 사라지지만, 여러 사람이 함께 꾼 꿈은 현실이 된다고 합니다. 캠퍼스에서 함께 꿈을 꾸며, 우리의 소중한 만남을 우연이 아닌 인연으로 만들어 준 서울대학교 기계항공공학부 시스템 건전성 및 리스크 관리 연구실 식구들에게도 깊은 감사를 드립니다. 각자가 마음속에 간직한 소망을 잃지 말고, 졸업한 후에도 세상에서 꼭 필요한 빛과 소금이 되기를 기원합니다.

저에게 가장 부족한 모습은 바로 부모님께 효도하는 것입니다. 더불어 여동생에게 제대로 해준 것이 하나도 없는 못난 오빠입니다. 그럼에도 불구하고 언제나 아가페적 사랑으로 든든한 버팀목이 되어준 가족에게 고백합니다. 여러분은 하나님께서 저에게 주신 가장 소중한 보물입니다.

만약 제 인생에 정릉청년교회와 JOY선교회가 존재하지 않았다면, 저를 향하신 하나님의 사랑을 결코 깨닫지 못했을 것입니다. 저를 말씀으로 양육해 주시고 기도로 섬겨주시는 모든 믿음의 동역자들께 감사의 말씀을 드립니다. 지금까지 살면서 넘치게 받았던 은혜를 갚을 수 있는 유일한 방법은 내 이웃들에게 그대로 흘려 보내는 축복의 통로가 되는 것이겠지요.

끝으로, 나를 부르신 길로 달려가도록, 나의 마지막 호흡이 다하도록, 나로 하여금 예수 그리스도의 십자가를 품게 하시니, 이 모든 것이 하나님의 한량없는 은혜입니다. 할렐루야!

본 연구는 2012년도 정부(교육과학기술부)의 재원으로 한국연구재단의 지원을 받아 수행된 기초연구사업(과제번호: 0420-20120048)이며, 이에 깊은 감사를 드립니다.